Aalborg University
Institute of Electronic Systems
Department of Health Science and Technology

TITLE:
Modelling Human Locomotion

THEME:
Biomedical Modelling

PROJECT PERIOD:
2002: September - December

PROJECT GROUP:
Group: 984

AUTHOR:
Pascal Theodoor Wolkotte

SUPERVISORS:
Francisco Sepulveda
Thomas Sinkjær
Mike Grey

EXTERNAL CONTACT:
Peter Veltink
University of Twente (NL)

NUMBER OF COPIES: 3
NUMBER OF PAGES: 67 pages
HANDED IN: 27 January 2003

ABSTRACT:

This report is a coverage of my 16 weeks practical training at the Center for Sensori-Motor Interaction of the Aalborg University (Denmark). One of their research topics is on the field of the biomedical modelling, where they want to answer the question of the functional behavior of the proprioceptive feedback system of the human body. A valid/good biomedical model could support their hypotheses which are results from different measurements.

The original intention of the project was to build a complete walking lower body model to find the reason for proprioceptive feedback during walking. In the middle of the project this original goal was a too high, because of the additional work of redesigning previous work of Huber [26]. The goal is adjusted to design the mechanical and muscle model and a well documented report, so a next project can continue immediately.

The mechanical and muscle model appeared to work correct and are verified with measured data. The forward activation of the muscle/mechanical model is not completely the same as expected. This is because the used method does not take co-activation of antagonistic muscle into account. For the continuation of this project a complete measured data set is necessary, because the verification is not 100% valid. This performed verification uses data that is not correlated in the sense that is measured at the same conditions and persons.

Contents

CHAPTER 1

Introduction

A practical training period is part of the Electrical Engineering master program of the University of Twente. This training could be at a company in the Netherlands or a university or company abroad. I chose to go to the Aalborg University (Denmark), which has a great reputation in educating and receiving international students. I contribute in a project at the Center for Sensory-Motor Interaction (SMI), which is a research group of the Health Science and Technology Department of Aalborg University. The project is under supervision of Thomas Sinkjær, Mike Grey and Francisco Sepulveda. This chapter is the introduction to problem and highlights the rest of the report.

About 7 million years ago at around the time of great climatic changes in the eastern Rift valley area of Africa, a transition to bipedal walking took place. At that time the first hominids appeared-bipedal primates who walked erect. Those early hominids were the ancestors of recent humans. What could have been the driving force behind this 2 legs walking instead of the normally 4 legs, like most of the animals still do. It must have been a strong stimulus, in view of not only the speed of transition, but also the additional control and balance difficulties imposed by bipedalism. Many anthropologists still cannot give a 100% accurate answer. Though still people are researching reasons for this behavior, at the SMI they are interested in helping people who have difficulties with walking due to for example a disease.

Researchers of the SMI are currently investigating the muscle afferent feedback during human walking. The major concern is to understand the functional importance of the neural pathways at different kinds of tasks. This research is the next step in order to understand the human locomotion. Other research projects investigated mainly cats and other quadrupeds to determine which neural pathways play an important role in walking. They concluded that sensory feedback from skin and moving muscles plays an important role in the locomotion.

One of these projects was realized by Arthur Prochazka and Sergiy Yakovenko [48] of the

university of Alberta (Canada). They investigated the behavior of the locomotion of cats. With a computer based model they modelled a various kinds of sensor systems and rules. This model is able to help with the question on the contribution of different subsystems to the walking pattern of cats.

Because of the time consuming and difficult tests of measuring many different types of movements of the human body, the question for this project was to make a computer model that could easily simulate the different types. Another problem is the difficulty of measuring individual nerves or nerve groups, because measuring only is possible on the skin. Some experiments could disable specific nerve groups, but that is a rather complicated test and not fully provable if all specific nerves are disabled. A computer model that could simulate many of these tests would be of great help. Other research groups made already simulations of the neural feedback, but all the signals are determined by a neural network [38]. A third area is only the activation of the muscle, which can be determined with inverse dynamics or trial and error of many possibilities [4].

This computer model should be able to help the researchers with changing the feedback path easily and look to the outcome of the walking pattern. After a little bit experience effects of changes should be visible. For example an opinion is that a person with epilepsy could have lower gains in the proprioceptive feedback (though other people think the opposite). With this model it is much easier to support this kind of hypothesis.

1.1 Project description

The original intention of this project was to answer the question:
- *What happens when part of the feedback is turn on and off?*
And the second question:
- *What happens if the feedback in partly turned on?*

Prochazka's suggestion is that cats using the feedback to change their muscle neural input for one phase (swing for example) to the next phase (stance in this case). At the SMI the idea is that in humans the neural feedback is directly affecting the neural input of the muscles. So it is not a discriminating but a regulating feedback. Setting up a model that can model the idea of continues feedback is the best option and makes clear if this will look familiar with a normal walking person.

When I started the information was I could use a already developed mechanical model. And I could put most of the time on the neural part. And before starting at the human model I should try to reproduce the work of Prochazka's walking cats. But the walking model of Prochazka is not available until their article is published.

The decision then was to continue on the human model and don't spend time on the cat model. But with a few weeks of work it became clear that the software package was not very suitable for modelling the ground contact forces, the model of Huber [26] was not correct and that calculation of the muscle forces is not so easy. That's the reason for not completing the complete project goal and it is adjusted to developing the right mechanical skeleton and muscle model.

With the models and report of this project a next person can have a flying start and continue with developing a good walking model.

1.2 Report index

Though it is only a small project, the report is quite large. The major reason for this choice is because the developed models are not finished to answer the important questions. The following project therefore can start more easily and has a better idea of all the choices made during this project.

This report starts with describing the physiological background in chapter 2. Before setting up the actual models different options for the subsystems are described in the modelling background of chapter 3. Because not much time is spend on the neural part only the ideas for neural models are described in this chapter. For the other subsystems also the implementation is described in chapter 4. Before the final conclusions and recommendations the validations of the models are described in the result chapter.

CHAPTER 2

Physiological background

2.1 Walking

Human walking or human gait gives people an picture of a cycling pattern. A description of walking therefore is confined to a single cycle. The assumption is that successive cycles are all about the same. Although this assumption is not strictly true, it is a reasonable approximation for most situations [15].

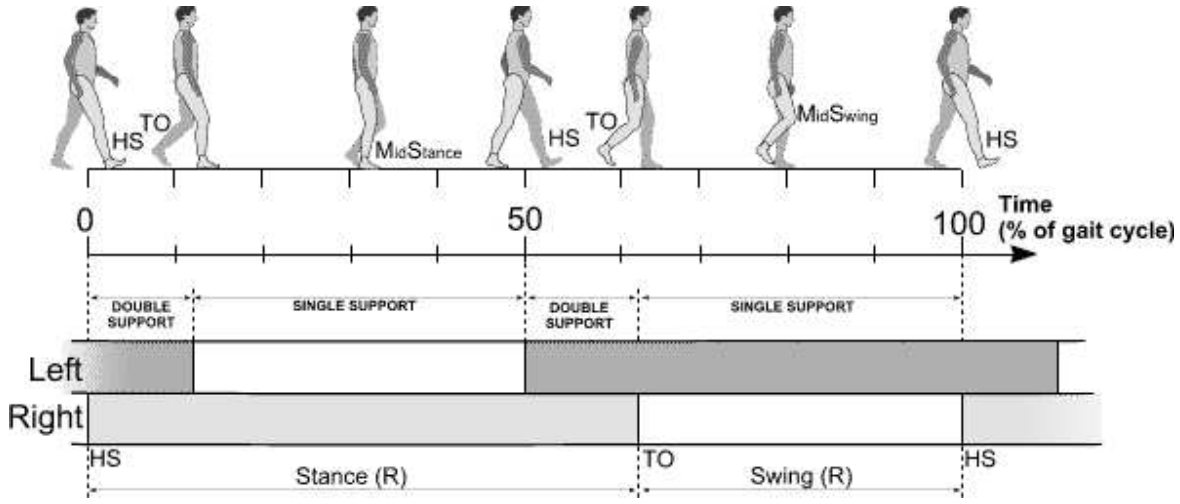

Figure 2.1: *A single walking cycle for a normal adult*

The basic walking cycle movements are divided into the times when the foot is on the ground (stance phase) and when the foot is off the ground (swing phase). Note that by convention,

the cycle begins when one of the feet makes contact with the ground, called heel strike. The period of stance and period of swing is speed dependent [22] [32]. For normal walking speeds ($\pm 1.5 m/s$ for an average man [40]) and patterns the these values lie between 60% and 70% for the stance phase and between 40% and 30% for the swing phase.

The other way of dividing human walking cycles is when both feet on the ground (double support phase) and when one foot on the ground (single support phase). The double support phase will decrease with the increase of walking speed [32]. At a certain speed the human will switch from walking to running, where swing time > stance time for both legs.

2.2 Muscles

The contraction specialists of the body are the muscles. The muscles are divided in three types:

- Skeletal muscles
- Cardiac muscles
- Smooth muscles

Through their highly developed ability to contract, muscle cells are capable of shortening and developing tension, which enables them to produce movement and to do work. This project discusses only the skeletal muscles, which are responsible for the movement of body segments.

2.2.1 Structure of skeletal muscles

Each person has about 600 skeletal muscles, which range in size from the delicate external eye muscles that control eye movements to the large, powerful leg muscles. All the skeletal muscles are striated and subject to voluntary control.

The muscle is covered by a sheath (= aponeurosis) of connective tissue that penetrates from the surface into the muscle to divide the muscle into columns or bundles. The connective tissue extends beyond the ends of the muscle to form though, collagenous tendons that attach the muscle to bones. A tendon may be quite long, attaching to bone some distance. These tendons have a white appearance and the central muscle part has a red or pinkish color.

A skeletal muscle consists of a number of muscle fibers (a single skeletal muscle cell). These muscle fibers are relatively large, elongated and cylinder-shaped, measuring from 10 to 100 micrometers in diameter and up to 750 millimeter in length.

Muscle fibers are oriented either in the direction of the tendon (i.e. a parallel fiber muscle) or at an acute angle α (=pennation angle) to the tendon (i.e. an unipennated muscle, see figure 2.2. More complicated pennated muscles exist and are illustrated in figure 2.3. This project assumes all the used muscle are modelled like a unipennated muscle and the α remains constant during contraction. But as for example discussed in [27] this gives not the best realistic description of a muscle.

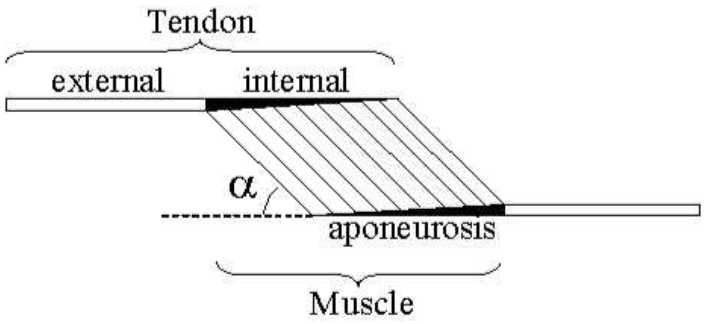

Figure 2.2: *Schematic model of an unipennated muscle. Coupling between muscle fibers and tendon in a pennated muscle. Muscle fibers lie in parallel to each other, have the same length and are oriented at the same angle α to the tendon. Muscle and tendon are linked together at the aponeurosis, or internal tendon. Modified from [61]*

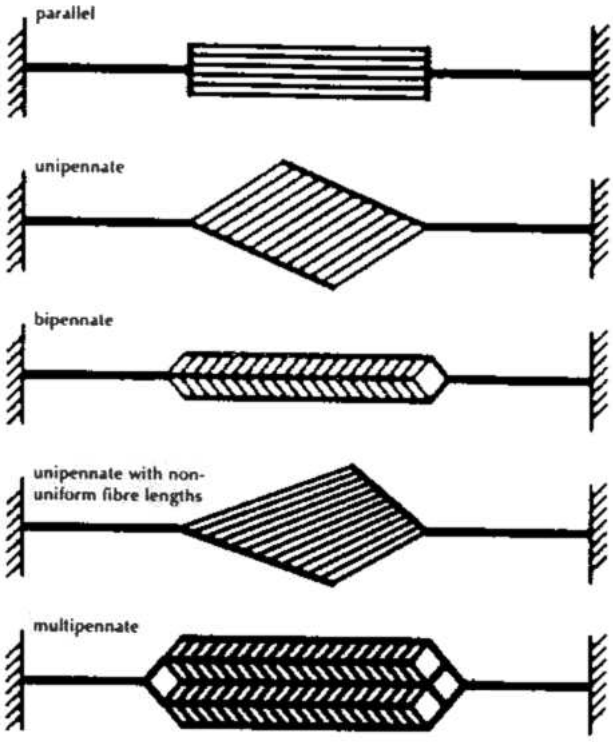

Figure 2.3: *Different muscle fiber configurations of pennated muscles. Taken from [17]*

2.2.2 Anatomy of skeletal muscles

The human skeletal muscle can be organized on different levels of organizations, see figure 2.4. The three major levels are explained in the next subsections.

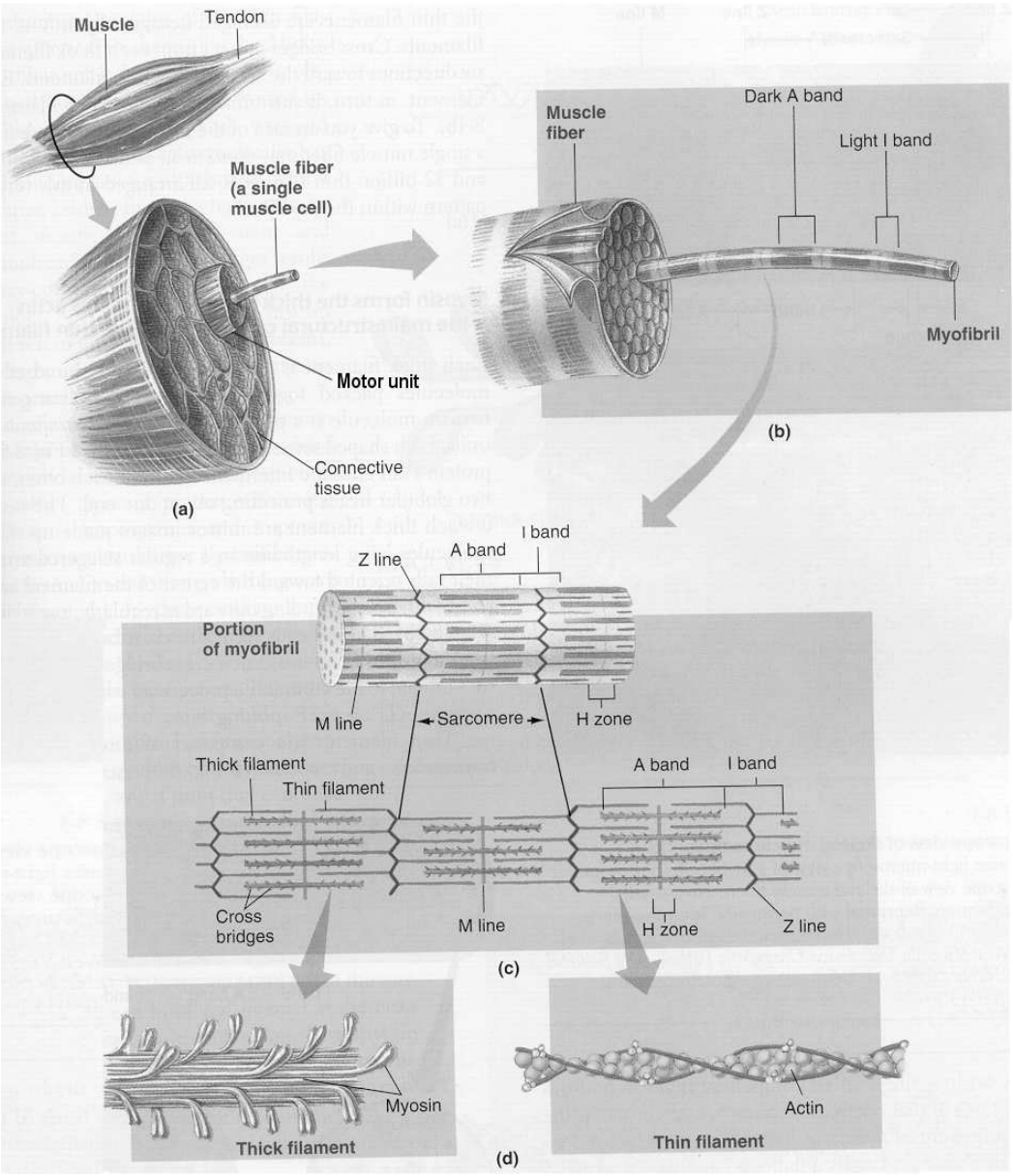

Figure 2.4: *The different levels of a muscle. Taken from [51]*

Motor unit

Each motor neuron that leaves the spinal cord usually innervates many different muscle fibers. One motor neuron plus all of the muscle fibers it innervates is called a motor unit. The muscle fibers that compose a motor unit are dispersed throughout the whole muscle. Thus their simultaneous contractions results in an evenly distributed, although weak, contraction of the whole muscle.

The total muscle contraction force occurs in two different ways:

1. By increasing the number of motor units contracting simultaneously. Small motor units are fare more easily exited than the large ones, and this effect the gradation of muscle

strength during weak muscle contraction to occur in a very small steps. The steps become greater as the intensity of contraction increases (the larger motor units begin to contract). A phenomenon known as motor unit recruitment.
2. By increasing the rapidity of contraction of individual motor units. Even though a single action potential in a muscle fiber produces only a twitch, contractions with longer duration and greater tension can be achieved by repetitive stimulation of the fiber. When a muscle is stimulated at greater frequency - strength of contraction is getting bigger. When the frequency has reached that point (critical frequency) at which the successive contraction fuse together, this state is called tetanization. Once the critical frequency for tetanization is reached, further increasing the stimulation frequency the force of the contraction increase only a few percent.

Muscle fiber

Based on the biochemical capacities, there are three major types of muscle fibers

1. Slow-oxidative (type I) fibers
2. Fast-oxidative (type IIa) fibers
3. Fast-glycolytic (type IIb) fibers

The difference between these types are: their speed of contraction and the type of enzymatic machinery they primarily use for ATP formations.

The speed of contraction depends on the speed of splitting ATP. The enzymatic machinery contributes in the speed of fatigue. With low oxidative glycolytic ATP the fatigue occurs very fast. The high oxidative type I and IIa have a higher fatigue resistance.

In humans, most of the muscles contain a mixture of all three fiber types; the percentage of each type is largely determined by the type of activity for which the muscle is specialized. The percentage differs not only between muscles within individuals, but also varies considerably among individuals. Most of us have an average of about 50% each of fast and slow fibers.

Myofibril

Every muscle fiber has a presence of numerous myofibrils. These specialized contractile elements are cylinder-shaped intracellular structures 1 μm in diameter that extend the entire length of the muscles fiber. Each myofibril consists of a regular arrangement of highly organized cytoskeletal elements, the thick and thin filaments.

The thick filaments, which are 1 to 18 nm in diameter and 1.6 μm in length, are special assemblies of the protein myosin, whereas the thin filaments, which are 5 to 8 nm in diameter an 1.0 μm long, are made up primarily of the protein actin. Under a microscope a myofibrils displays alternating dark bands (A band) and light bands (I band). An A band consists of a stacked set of thick filaments along with the portions of the thin filaments that overlap on both ends of the thick filaments.The I band consists of the remaining portion of the thin filaments that do

not project into the A band. In the middle of each I band is a dense, vertical Z line. The area between two Z lines is called a sacromere, which is the functional unit of skeletal muscle.

2.2.3 Contraction of skeletal muscles

Binding of actin and myosin molecules at the cross bridge results in energy-consuming contraction of the muscle fiber. In a relaxed muscle fiber, contraction does not take place, actin is not able to bind with cross bridges because of the position of the two other type of protei within the thin filament- tropomyosin and troponin. Tropomyosin molecules are threadlike proteins that lie end to end alongside the groove of the actin spiral.

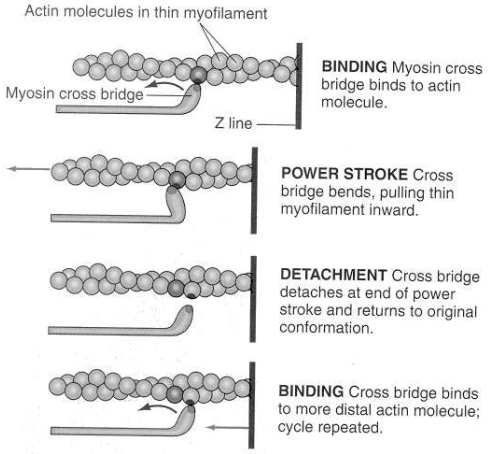

Figure 2.5: *Schematic view of the contraction of a sacromere*

In this position, tropomyosin covers the actin sites that bind with the cross-bridges, thus blocking the interaction that leads to muscle contraction. When Ca2+ binds to troponin, the shape of this protein is changed in such a way that tropomyosin is allowed to slide away from its blocking position. With tropomyosin out of the way actin and myosin can bind and interact at the cross bridges, resulting in muscle contraction. The motion of the myosin heads requires energy (ATP) but it is still not known exactly how ATP is used to provide the energy for contraction. The concentration of ATP in the muscle fiber is sufficient to maintain a contraction for few seconds, so the sources of energy to reconstitute the ATP are: phosphocreatine and the energy released from foodstuffs - fats, proteins and carbohydrates.

This muscle contraction is performed in small steps stepping the myosin cross bridge along the cross-bridge binding site of the actin molecules. At any time during contraction, part of the cross bridges are attached to the thing filaments and are stroking, while others are returning to their original conformation in preparation for binding with another actin molecule.

Initiation and prolongation of Muscle Contraction

The skeletal muscle fibers are exited by nerve fibers attached to the muscle fibers at neuromuscular junction. Initiation of contraction in skeletal muscle begins with action potentials which

are transferred from these nerve fibers to muscle fibers.

1. An action potential will release Acetylcholine(ACh) from the terminal of a motor neuron. This ACh initiates an short action potential in the muscle cell that is propagated over the entire surface of the muscle cell membrane.
2. The surface electric activity is carried into the central portions of the muscle fiber via the transverse tubules cause release of Ca^{2+}-ions from the sarcoplasmic reticulum
3. The Ca^{2+}-ions initiate the chemical events of the contractile process as described in the previous section
4. The process of binding, bending, detachment will continue as long as Ca^{2+}-ions are present outside the sarcoplasmic reticulum. The Ca^{2+}-ions is actively returned to its storage site in the sarcoplasmic reticulum's lateral sacs by calcium pumps.

Time constants of Muscle Contraction

Although a single action potential in a skeletal muscle fiber lasts only *1 to 2 msec*. The onset of the resultant contractile response lags behind the action potential because the entire excitation-contraction coupling process must take place before cross-bridge activity begins. The action potential is completed before the contractile apparatus even becomes operational. This time delay of a few milliseconds is known as the *latent period.*

Time is also required for the generation of tension within the muscle fiber produced by means of the sliding interactions between the thick and thin filaments through cross-bridge activity. The average contractile time is between *15 and 50 msec* and depends on the type of muscle fiber. This contractile response does not cease until the lateral sacs have taken up all of the Ca2+ released in response to the action potential

After all the Ca2+ is removed, it takes time for the filaments to return to their resting positions. This relaxation time usually lasts slightly longer (between *25 and 60 msec*) and is also depend on the type of muscle fiber.

Types of contraction

In a physiological view the muscle contracts on two basic conditions, isotonic and isometric. An isotonic contraction occurs when the muscle develops a constant force and the muscle shortens (concentric) or lengthens (eccentric) depending of the external force. In an isometric contraction the length of the muscle is constant and the muscle produces a certain force at a constant length. Isotonic take care of the movement of body parts as isometrics is more for posture tasks or hold a object at a certain height. Of course a specific task can require a combination of the two contractions.

The same internal events occur in both isotonic and isometric contractions: the tension-generating contractile process is turned on by muscle excitation; cross bridges start cycling and filament sliding shortens the sarcomeres, which stretches the series -elastic component to exert force on the bone at the site of the muscle's insertion.

2.2.4 Receptors of skeletal muscles

Skeletal muscles are richly supplied with a variety of receptors. Two receptors are particularly important form motor control: the muscle spindles and the Golgi tendon organs. These 2 receptors are innervated by group I (large myelinated) and group II (small myelinated) afferent fibers.

Muscles Spindles

There are 25000-30000 muscle spindles in the human body, including about 4000 in each arm and 7000 in each leg. Muscle spindles are encapsulated structures, ranging from 4 to 10 mm in length. Each spindle has three main components: a group of specialized muscle fibers, sensory axons that terminate on the muscle fibers and γ-motor axons that regulate the sensitivity of the spindle (figure 2.6). The center of the spindle is enclosed by a connective tissue capsule filled with a gelatinous fluid that facilitates sliding of the muscle fibers with in it. Thus, the spindle is slightly swollen in the center, and the ends are tapered, giving it fusiform or spindle like shape.

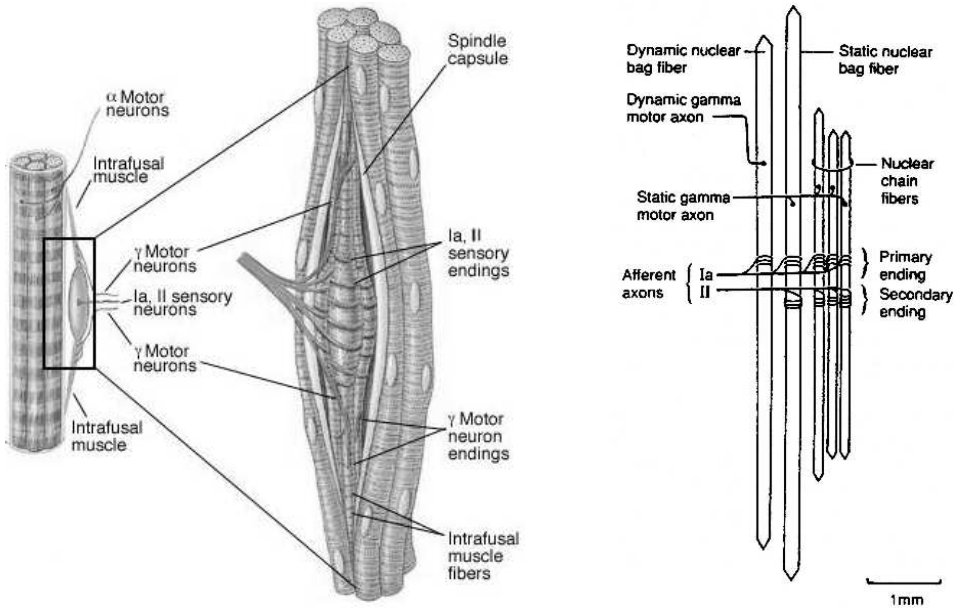

(a) Physiological (b) Model

Figure 2.6: *Muscle spindle. From [31]*

The specialized muscle fibers of the muscle spindle are called interfusal fibers to distinguish them form ordinary skeletal muscle fibers, the extrafusal fibers. Intrafusal fibers are smaller than extrafusal muscle fibers and do not contribute significant force to the muscle contraction. Three types of intrafusal muscle fiber can be distinguished per typical mammalian muscle spindle:

1. $\pm$5 Nuclear chain fibers
2. 1 Static nuclear bag fiber
3. 1 Dynamic nuclear bag fiber

The different properties of the three types of interfusal fibers play a major role in determining the firing characteristics of the sensory endings of the spindle.

The interfusal fibers receive their input from fusimotor axons. The fusimotor axons are divided in static and dynamic γ-motor neurons. Sometimes the fibers also receive input from a β-skeletofusimotor axon, which also innervates neighboring extrafusal fibers. The effect of the fusimotor action on fiber characteristics is widely investigated. In general the terms dynamic and static fusimotor are in fact misleading, in that both types alter mainly the gain and offset rather than the dynamics of the sensory endings responses to stretch [42].

There are two types of sensory endings in muscle spindles: primary and secondary. There is usually just one primary ending in each spindle, consisting of all the branches of a single group Ia afferent axon. Group Ia afferents terminate on all three types of intrafusal fibers. There is also usually one secondary ending in a spindle consisting of the terminations of a single group II afferent. The group II fibers terminate only on chain fibers

The length-response characteristics of spindle primary and secondary endings with and without fusimotor action have been characterized in great detail over the last 50 years. The basic spindle characteristics are remarkably similar in cats, monkeys, and humans [42]. In absence of fusimotor action both Ia and II endings transduce length changes dynamically. The Ia endings have a larger velocity- and acceleration sensitive components of response. The II afferents are more sensitive to low displacements and velocity. This give the muscle spindles a continuum of behavior. The non-linear aspects of response is caused by the the stretch sensitivity that depends on amplitude, offset and after-effects of muscle and fusimotor contraction. The sensitivity also depends on the non-linear velocity scaling.

Golgi Tendon Organs

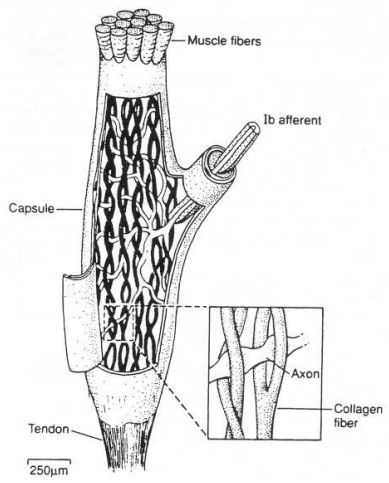

Figure 2.7: *Golgi Tendon Organ*

Golgi tendon organs are slender encapsulated structures about 1 mm long and 0.1 mm in diameter. They are typically located at the junction of muscle and tendon, where collagen fibers

arising form the tendon attach to the end of groups of extrafusal muscle fibers. They are therefore connected in series to a group of skeletal muscle fibers. (see figure 2.7)

Each tendon organ is innervated by a single group Ib axon that loses its myelination after it enters the capsule and branches into many fine endings, each of which intertwines among the braided collagen fascicles. Stretching of the tendon organ straightens the collagen fibers. This compresses and elongates the nerve endings and causes them to fire. Because the free nerve endings intertwine among the collagen fiber bundles, even very small stretches of the tendon organ can deform the nerve endings. This make the tendon sensitive to even a few 1 μN. The firing rate of tendon organs is very sensitive to changes in tension of the muscle. Tendon organs stretch most easily when the muscle tension increases due to contraction.

CHAPTER 3

Modelling background

Setting up a model of a certain system requires a global overview of this model. With information of differen t books a structural diagram is created like in figure 3.1. This figure contains all the main structures/signals in the human leg necessary for the movement of the body and of course also the necessary environment. In the next sections the three indicated models are described, with respect to what already is investigated by others and found in literature. It will give the basis for the choices made in this project.

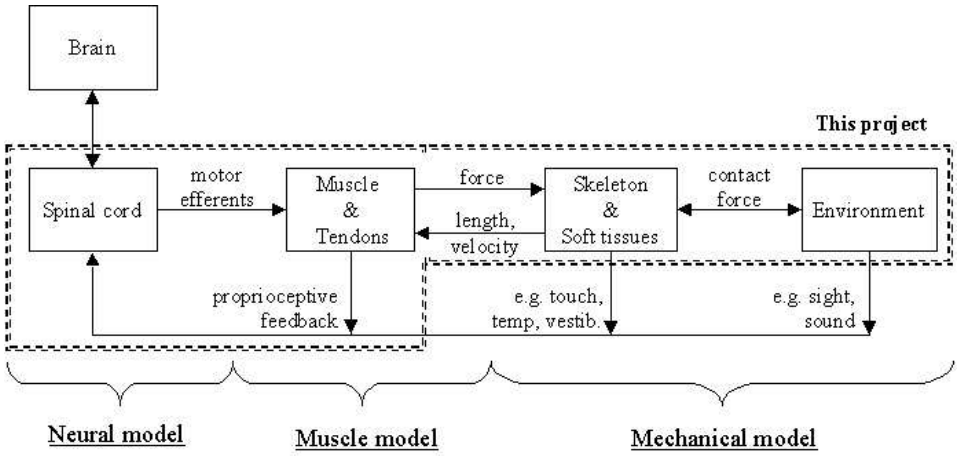

Figure 3.1: *Structural diagram of movement control system. Each of the blocks in the diagram represents a physiologically identifiable part of the system*

3.1 Mechanical model

The mechanical part of the model contains all systems, which can be (completely) characterized with mechanical quantities like mass, center of gravity, position and inertia. First there is the interaction between the human and the environment. This is mainly due to the gravity and contact with the ground. The gravity is very simple to divine, but for the ground contact more information is given in the next subsection. The system between the muscles and environment is divined by the skeleton and soft tissues and is described in the subsection anthropometry of the skeleton. Then there is the choice between a 2D or 3D model, which is highlighted in subsection 3.1.3. The last subsection discusses the connection points of the muscles on the skeleton, which creates the link between the muscle model and mechanical model.

3.1.1 Ground contact

As mentioned in section 2.1 on page 5, $\pm 60\%$ of a walking cycle there is ground contact with one or more areas of the foot. But $\pm 40\%$ of the cycle the foot is free from the ground. A model of a walking human therefore requires a model of the ground that prevents the foot from falling below the ground level, but also is able to release the foot from the ground at toe-off.

The contact between two bodies (foot/human and ground/earth) is in principle the reaction of 2 inertia's. When a simulation program has no collision detect, the main solution for calculating the reaction force is with use of a spring and damper in the vertical and horizontal plane. For example Ogihara and Yamazaki [38] or Silva and Tenreiro [52] model the ground contact with 2 viscoelastic elements at the heel and at the toe, like in figure 3.2. The parameters for the spring and dampers differ between the mentioned articles.

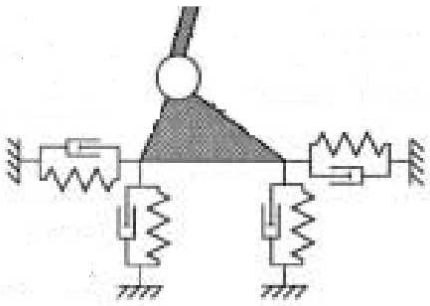

Figure 3.2: *Ground contact model to prevent the foot from sinking into the ground*

Anderson and Pandy [4] model their ground with a series of spring-damper units distributed under the sole of each foot. Four ground springs were located at the corners of the hind-foot segment, and one was positioned at the distal end of the toes.

Another option is described by Pop et al. [39] and it uses the center of pressure (COP) of the foot to apply the ground reaction force. It is a simplified representation of figure 3.2 and prevents an over-constraint system. Their ground reaction force should be equal to forces of figure 4.11 in Winter [56].

3.1.2 Anthropometry of the skeleton

The mechanical part of the project is the design of the skeletal system and its necessary simplifications. A human has an enormous amount of joints, bones and soft tissues. Only in one lower leg 30 bones and 38 individual muscles can be identified. Every two bones connected with each other will have between 1 and 6 degrees of freedom, therefore a simplification is necessary for a first model. The most common method is combining bones into segments. This starts with 1 segment for the whole body, via 3 segments (HAT, a thigh and a shank) to a specific number of segments. The most common option is to define a 7 segment human model with a thigh,shank/calf and foot per leg and a segment for the head, trunk and arms (HAT). According to Popovic and Sinkjær [40] 3 other options are: separating the pelvis from the trunk, modelling the foot as multiple segments and a 13 segment body model with a splitting up the HAT.

For modelling the lower leg segments, there are different approaches to estimate the real mass, inertia, center of gravity (=CG), and length for a correct mechanical model. The mass, inertia, length and shape of the different bones, muscles and soft tissues can be combined, because there is no need to model the individual muscle mass. The different segments (HAT, thighs, shanks and feet) can be modelled like rigid segments.

A widely used method is describing the calf and thigh like a cylinder and the foot like a pyramid. The inertia-parameters are calculated with known formulas for these shapes. The mass and length parameters can be calculated with the use of Winter's chapter 3 [56]. But according to Vaughan et al. [15] a more precise representation is possible by adding a many anthropometric parameters. Their anthropometric model is validated with measurements on 6 cadavers.

3.1.3 2D or 3D?

A human body can be divided in three primary planes: sagittal, coronal (or frontal), and transverse (see figure 3.3). Most researchers on modelling the human locomotion emphasize the sagittal plane and ignore the other two. The main reason for this is to have a simple 2D model of the human and a reduced number of degrees of freedom. But for example the ankle inversion and eversion can not be modelled in a 2D model, because than a semi- or full 3D model is necessary.

In analyzing the kinetic data already more researchers look to all the three planes (or in 3D). Vaughan [15] for example give the movement of the lower legs in all the three planes. The main reason for this is: With analyzing there are certain pathologies where another plane (e.g., the coronal, in the case of bilateral hip pain) would yield useful information.

3.1.4 Muscle line of action

A muscle line of action is defined as a straight or curved line along which the muscle force is acting. The muscle force is the result of summation of the contribution of all individual muscle fibers. This line of action will determine the moment arm and direction of the force. Hence,

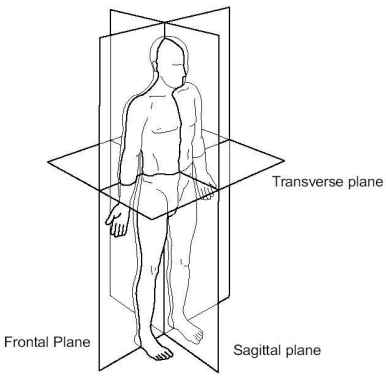

Figure 3.3: *The three human planes. From [15] and original from [30]*

assuming one muscle line of action is already a simplification. Representing a whole muscle body, by for example using finite element models, is on the other hand a very time computation time consuming operation.

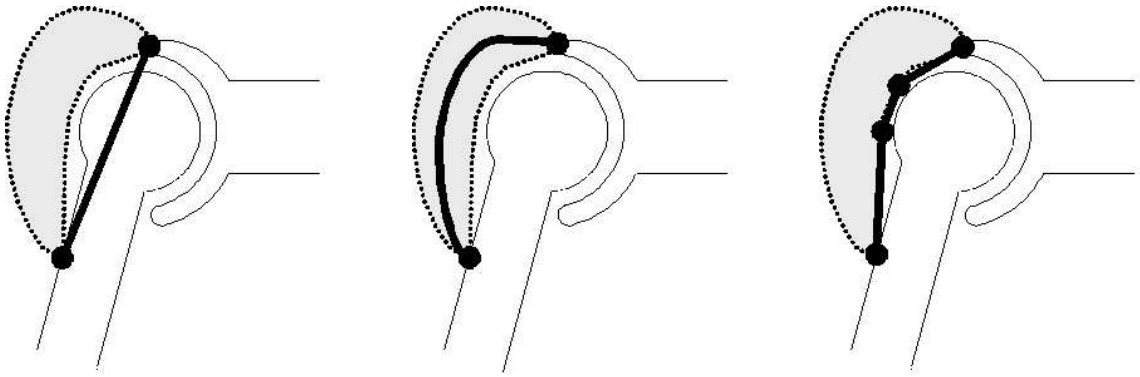

(a) Straight line (b) Centroid line of a muscle (c) Wrapped line

Figure 3.4: *3 Different ways of modelling the muscle line of action. The grey area is the muscle/tendon body and the black line is the modelled line of action*

The simplest way of modelling the muscle line of action is by a straight line from origin to insertion. However, for some muscles this is an impermissible simplification (see figure 3.4a). Another approach is to determine the centroid line of a muscle, which is the central line through the muscle belly (see figure 3.4b). But problem with this approach is that the direction of the muscle force is still unknown. A force acting along a curved line will generate reaction forces at the structure underneath, which must be known for a force equilibrium. A third approach is to use the bone contour, around which the muscles are wrapped (figure 3.4c).

The last option is used in the muscle modelling program SIMM [16], where the muscles curve around a pre-divined shape. In the the inverse dynamics program Anybody, the muscle goes through pre-divided rings, called via-points. It is a comparable solution as in SIMM, but nog exactly the same.

For muscles with large attachment sites, one muscle line of action is not sufficient to represent

the mechanical effect of the muscle. Usually, these muscles are split in small muscles with all one line of action.

3.2 Muscle model

The mechanical muscle modelling is a widely investigated area. Most muscle models typically contain three elements (see figure 3.5). Another option could be a complete black-box of the muscle. But this will require a good training set. This also will not gain extra information of inside muscle behavior, which maybe will be necessary in the future.

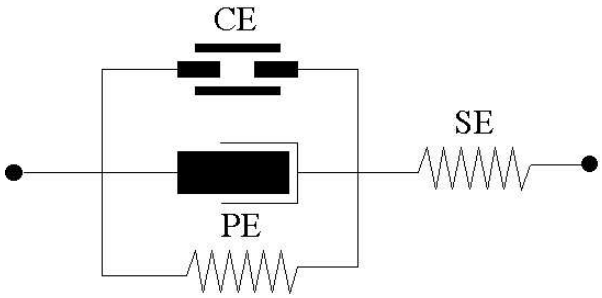

Figure 3.5: *Basic muscle model structure*

The parallel (visco-)elastic element (=PE) models the force generated by the fascicles under passive conditions. In figure 3.5 it consists of a damper and a stiffness. This damper is not always present. The contractile element models the active contractile machinery force of the muscle. This force is transmitted through the series elastic element (=SE) to the point of attachment. The SE models the series elasticity of the tendon and aponeurosis. The combination of the contractile and (visco-)elastic elements is referred to as the muscle-tendon-unit.

There is another widely used muscle model, where the PE is parallel to both the CE and SE. Because the SE is much stiffer than PE over the primary operating range, it almost does not matter which form is used.

The implementation of the series and parallel elastic element differs from model to model. But the general implementation is a (non-)linear spring with a limit operating range. The implementation of the contractile element is a more complex part of the model. It therefore will be explained in the next subsection. In subsection 3.2.2 the anthropometry of the muscle is described and this section ends with a section about the proprioceptive feedback. All the mathematical relations of the muscle model in this project are discussed in section 4.5 and Appendix B.

3.2.1 Contractile element

There are two types of contractile element models. One is empirical, build on the work of Hill [21]. The other is more structural, and based on cross-bridge kinetics as formulated by Huxley [28].

The Huxley models are based on the structure and chemistry on the muscle. For example, Zahalak [60] investigated the model and he developed a structural model describing excitation-contraction coupling and contraction dynamics. The model is a 5th order model for one motor unit. This is not suitable for modelling a complete multi-joint model, because it would result in a too high order model.

The Hill-based contractile element models are based on a more black-box approach. The normalized output force is the product of three independent experimentally measured factors. The factors describe the force-length property ($= FL(l_{muscle})$), the force-velocity property ($= FV(\dot{l}_{muscle})$) and the activation dynamics ($= AD(u_{neural})$) of the neural input. All the three factors and CE-force are normalized to the maximum muscle force at optimal muscle length ($= F_o$).

$$F_{CE} = AD(u_{neural}) \cdot FL(l_{muscle}) \cdot FV(\dot{l}_{muscle}) \tag{3.1}$$

More information about the three factor is described in the next sections

The popularity of Hill-based models is based on its structure[1]:

1. The multiplicative structure captures the major nonlinearity of the muscle, which is the scaling of static and dynamics properties by each of the three factors.
2. The three individual factors an their parameters describe familiar and intuitive concepts that have been well verified.
3. The parameters for the force-velocity and force-length properties can be related to the sacromere structure.
4. The single scalar neural input is analogous to the EMG.
5. The model is computationally simple.
6. Although the model certainly does not capture all known behavior, it could easily be extended with particular properties if they are important in certain situations [57].

Force-length relation

In a Hill-based model the force-length relation describes the reduced muscle force, when a muscle is not at his optimal working length ($= l_o$). An example of this curve is presented with a simple equation:

$$FL(l_{muscle}) = -6.25 \cdot (\frac{l_{muscle}}{l_o})^2 + 12.5 \cdot (\frac{l_{muscle}}{l_o}) - 5.25 \tag{3.2}$$

The maximum working range of a muscle is roughly between $0.6 \cdot l_o$ and $1.4 \cdot l_o$. For this range the FL-curve of eq. 3.2 is visible in figure 3.6.

[1] List from Crago [13])

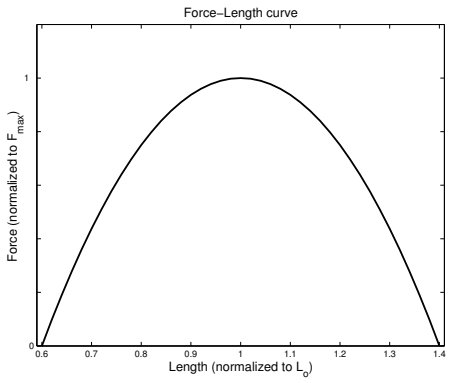

Figure 3.6: *Normalized Force-Length relationship. From Epstein and Herzog [17]*

Force-velocity relation

In the work of Hill [21] he introduced his famous original model consisting of a contractile element and a serial elastic element. From the study of heat production in a muscle he concluded that shortening can be divided into two parts: an instantaneous shortening and a constant velocity shortening. The instantaneous shortening was attributed to the serial elastic element. The constant velocity shortening resulted in a formula known as the Hill hyperbola (plotted in right-side of figure 3.7):

$$FV(\dot{l}_{muscle}) = FV(v_{muscle}) = \frac{F_o(l_{muscle})b - a \cdot v_{muscle}}{b + v_{muscle}} \tag{3.3}$$

For the maximum velocity (v_{max}), the force becomes zero, so from eq. 3.2 we can deduce that $F_o \cdot b = a \cdot v_{max}$. For many muscles across species and temperatures a constant of 0.25 was found for $a/F_o = b/v_{max} = 0.25$.

For the elongation of the muscle force the muscle is able to produce more than the F_{max}. Typical values for the force produced with an elongated muscle are between F_{max} and $\pm 1.55 \cdot F_{max}$ and have a curve-shape like in the left-side of figure 3.7.

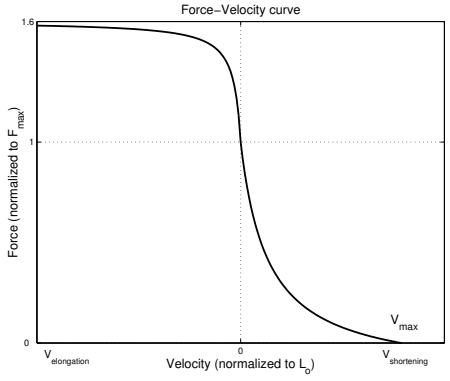

Figure 3.7: *Normalized Force-Velocity relationship. From Epstein and Herzog [17]*

Activation dynamics

This part of the contractile element is the most difficult part to describe in a simple muscle model. A brief description of a few solutions are given.

According to Winters and Stark [59] this part of the muscle model should represent the neural excitation-relaxation of the neural input by a linear first-order model. It describes the filtering of (infinite bandwith) neural input. The output of this block almost equal to measured EMG. Then the EMG should go trough an activation-deactivation block, which is described by a non-linear first-order model.

Van der Helm and Rozendaal [54] model the activation dynamics by a second order low-pass filter. The time constant of this second-order filter are 0.04 sec for the muscle excitation and 0.03 sec for the muscle activation.

Brown and Loeb [6] describe a more accurate model of the activation dynamics. They measured the FL-curves at different activation levels (see figure 3.8a). The FL-curves at different stimulus frequencies are not congruent. The effects of filament overlap were removed in the data set by normalizing the forces to the tetanic data. This revealed strong length dependencies of activation that were independent of filament overlap (see figure 3.8b).

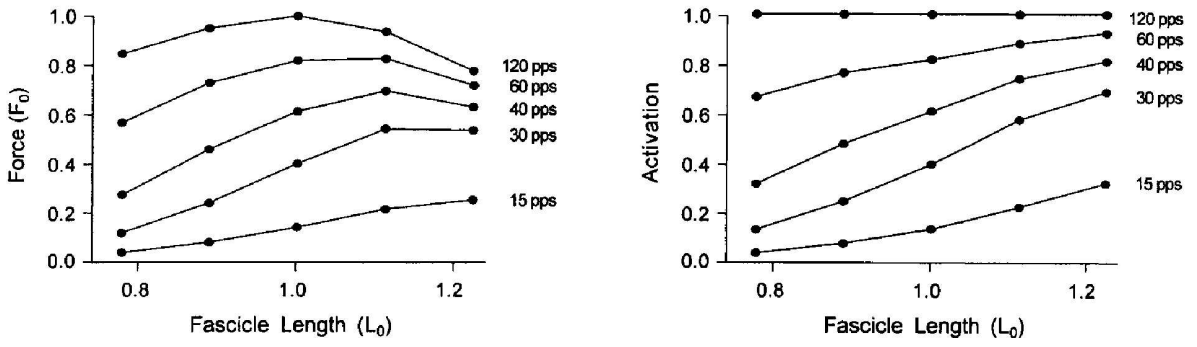

(a) FL-curve (not normalized)

(b) FL-curve (normalized to the tetanic data)

Figure 3.8: *FL-curve for different activation levels. From Brown and Loeb [6]*

With a change in axes the figure 3.8b changes into figure 3.9 together with the model that fits this data. The activation level is normalized to the level measured at half of the optimal muscle force ($0.5 \cdot F_o$) at optimal fiber length (l_o).

The activation dynamics also have characteristics known as sag and yield, which are also described by Brown and Loeb in [8]. This article and the previous mentioned belong to a series describing many different aspects of the mammalian muscle model ([7], [6], [9], and [8]).

3.2.2 Muscle/tendon anthropometry

In the previous sections different methods for calculating the muscle force are mentioned, but these forces are all normalized to maximum muscle force(F_{max}) at optimal muscle length (l_o).

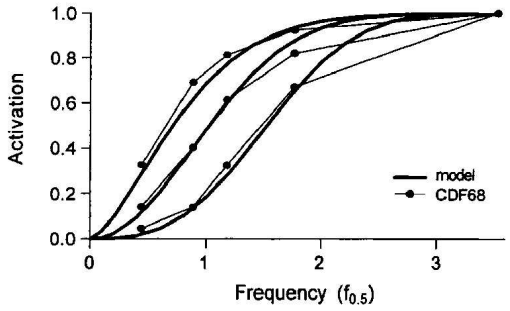

Figure 3.9: *Together with the points of figure 3.8b the suggested model of Brown and Loeb [6] is visible. Increases in length shifts the Af relationship to lower frequencies. From [6]*

To calculate the force of a specific muscle these parameters the muscle has to be found. The optimal fiber length normally is measured with a total relaxed muscle, so a cadaver study is able to find these lengths. Measuring the maximum force for all the individual muscles is very difficult, because it is hard to isolate one muscle at a time.

A more used method is by relating the muscle and muscle/tendon force to the Physiological Cross-Sectional Area (= PCSA). The PCSA is a measure of the number of sarcomeres in parallel with the angle of pull of the muscles. In parallel-fibered muscles the PSCA [cm^2] is:

$$PSCA = \frac{m}{\rho \cdot l} = \frac{V}{l} \tag{3.4}$$

And for pennated muscles:

$$PSCA = \frac{V \cdot \cos(\alpha)}{l} \tag{3.5}$$

where: m = mass of muscle fibers [$gram$]
ρ = density of muscle [$gram/cm^2$]
l = length of muscle [cm]
V = volume of muscle [cm^3]
α = pennation angle (see figure 2.3 on page 7 and figure 4.14 on page 44)

To determine the specific muscle force the PCSA has to be multiplied with a stress value (k):

$$F_{max} = k \cdot PSCA \tag{3.6}$$

A wide range of stress values for skeletal muscles has been reported [56]. But Delp et al. [16] calculated these forces for all lower extremity muscles with a constant factor around the 60 N/cm^2 (exact value is not mentioned in the article). Their sources for the PCSA where [55] and [5] and used for the stress factor the value from [53].

3.2.3 Proprioceptive feedback

As mentioned in the previous chapter on page 12 the 2 main sensors that measure muscle force, length, velocity and acceleration are the GTO's and muscle spindles. The problem is that there

is almost no information of model characteristics of these human organs. Most of the research is done on cats and other animals. In the next sections different suggestions for modelling these sensors are based on research on cat muscle and are validated with cat locomotion.

Although in this project no time is spend on finding an analogy between human and cat information, the first idea was to change only the gain in the equations 3.7 and 3.10. This is suggested by Prochazka [43], because the firing rate of human muscle afferent nerves appear to be lower than firing rates measured on walking cats. The second option mentioned in the same article is the difference in relative muscle velocities between cats and human, which has a direct influence on the firing rate. The last possible difference is more prominent effect of the α/γ linkage.

Muscle spindles

Various mathematical models of the the Ia muscle spindle have been developed. Though it has always been recognized that nonlinearities are a major problem, several very useful linear frequency-response analysis have been published by Chen and Poppele [11], Matthews and Stein [37], and more are mentioned in [42]). However, a limitation of the linear models is that velocity-sensitive components of the Ia responses to ramps do not scale with increasing velocity. A power-law relationship between Ia responses and velocity stretch is proposed by Houk et al. [23], Schäfer [50], Hasan [18], and more are mentioned in [42].

The predicting accuracy of previous mentioned models for Ia afferents are evaluated for cats by Prochazka and Gorassini [47] and [46]. All of the Ia models ([11], [37], [23], [50], [18]) predicted fitted the chronic data well. However, when the same models are tested on Ia responses to slow ramp-and-hold stretches some predicted the responses better than others. The model of Hasan (eq. 3.7) appears the best overall choice. And even though linear model of Chen & Poppele (eq. 3.8) does not have an explicit length-dependent term, its low frequency sensitivity appears to suffice for all but the slowest movements. It therefore is a second usable model to predict firing rates.

For the II afferents there is not so much information. Poppele and Bouwman (eq. 3.9) [41] suggested a comparable linear function for the II afferent as for the Ia afferents (eq. 3.8). Prochazka [43] added extra EMG and offset information to this function.

$$Ia_{firingrate} = 4.3 \cdot velocity^{0.6} + 2 \cdot displacement + K_{EMG} \cdot EMG + meanrate \tag{3.7}$$

$$Ia_{firingrate} = \frac{K_{Ia} \cdot s \cdot (s+0.4) \cdot (s+11) \cdot (s+44)}{(s+0.04) \cdot (s+0.8)} \cdot displacement^2 \tag{3.8}$$

$$II_{firingrate} = \frac{K_{II} \cdot (s+0.4) \cdot (s+11)}{(s+0.8)} \cdot displacement \tag{3.9}$$

Although the gamma motor neurons are called the *static* and *dynamic* fusimotor action, but they do not changes the dynamics behavior of the spindles. They mainly change the gain and offset

[2]The term s+11 is replace with s+4 when the displacement inputs are smaller than 0.5% of the rest-length [11]

of the Ia and II afferents. So the gamma-action changes the K levels in equation 3.8 and 3.9 ($\gamma_{dynamic}$: increased K_{Ia} and γ_{static}: decreased K_{Ia}, increased K_{II}) [42]. The influence of the gamma motor neurons on equation 3.7 is not found.

Golgi Tendon Organs

According to Prochazka [42] Golgi Tendon Organs have similarities with the II muscle spindle afferents. They both have a high-pass filtering property and tend to fire fairly regularly. A linear transfer function is suggested by Houk and Simon [24] (eq. 3.10) and discussed by Prochazka [43].

$$Ib_{firingrate} = \frac{K_{Ib} \cdot (s + 0.15) \cdot (s + 1.5) \cdot (s + 16)}{(s + 0.20) \cdot (s + 2) \cdot (s + 37)} \cdot force \tag{3.10}$$

But the Ib afferent have also a various sources of nonlinearity [42]:

- Ib endings may be unloaded by contractions of muscle fibers not inserting into the receptor capsule.
- The relationship between whole-muscle force and the force produced by the tendon organ's motor unit is unlikely to be perfectly linear.
- Each new recruited motor unit will cause a characteristic step in firing rate and are called the beating effect.

3.3 Neural part

Due to extra performed work in other parts of the model the neural part is not reviewed that extensively. Only a few discussions have taken place with the supervisors and the result of this is mentioned below.

3.3.1 Central Pattern Generator

The main discussion about a Central Pattern Generator (CPG) is de existence and where it is located. The general idea is presence of a central pattern generator (needed for walking) somewhere in the spinal cord or brain. Research with cats showed a CPG in the central nerve system is present. A best proof is a spinalized cat on a treadmill. The animal creates a repeating pattern, which looks quite similar to a normal walking pattern. With this pattern the cat is able to walk (stable). The same behavior for humans is not shown, because an adult is not able to walk after a spinialization of his spinal cord. Though a research with young baby's (not able to walk) gave the same results as cats on a treadmill. The EMG of the baby's showed the same repeating pattern as measured from young children. By now this is the best evidence for a CPG in humans.

The first idea was to implement a "CPG" in the spinal cord of the human model. Though this is not a complete realistic description. In combinations with the article of Hof et. al [22] this CPG can be speed independent. Two basic patterns/muscle can generate a activation pattern with the right settings for a certain speed.

3.3.2 Signal data-paths

Between the blocks: muscles and spinal cord (see figure 3.1) is a signal path and of course also for the afferent path. These path consists of a single nerve/muscle part, without any synapses. The transfer time for the nerve signals depends on the length and conduction velocity of the nerve. The length of the nerve depends mainly on the position of a muscle and a little bit on the starting position in the spinal cord (almost equal for the lower leg nerves). The velocity depends mainly on the diameter of the nerve and the myelinization. No research is further performed on this topic. A third problem is the distribution of the afferent nerves over a muscle, which gives different transfer times. The last "unknown" transfer time is synapse transfers and number of interneurons. Both will give an extra delay, which also differs between nerves and muscles

3.3.3 Feedback paths

Like in a control engineered model the sensor information is feedback to the intentional input and subtracted. This will result in a better/stable system. For many years the general idea in the biomedical world the same principle is used for the proprioceptive feedback . But in the last few years there research on cats is performed by Prochazka at al. ([45] and [44]) and they showed that also a positive force feedback gives a stable system within a certain operation range. The reason for this was the delay that is caused by the nerve-fibers and in the spinal cord by interneurons. A delay has a stabilizing effect with positive feedback. In a negative feedback a delay results in a more unstable behavior.

An extra problem is change in sign with cats when they change form a task. For example the force-feedback seemed to be negative or almost zero at posture tasks, becomes positive during walking.

CHAPTER 4

Implementation

This chapter describe the implementation with reasons of the different systems in this project. Before the actual implementation a number of choices had to be made. These choice are given in the first section. After the choices it was possible to get the necessary data-sets. After all this pre-work the actual mechanical and muscle model could be constructed, which is available in the last 2 sections. Because there was no time to implement the neural part it also is not available in this report.

4.1 Muscle choices

In this project the focus was on activating the lower leg muscle to generate a walking movement. It could be useful to model all the possible lower leg muscles [4], but with the main reason of simplification a choice of 6 lower leg muscle was necessary.

- Tibialis Anterior
- Soleus
- Gastrocnemius[1] (Lumped muscle of Gastrocnemius medial head and lateral head)
- Vasti[1] (Lumped muscle of vastus medialis, lateralis and intermedius)
- Hamstrings[1] (Lumped muscle of biceps femoris long head, semimembranous and semitendinosus)
- Rectus Femoris

The major reason to chose for the mentioned 6 muscle were:

[1] If muscles had the same function and almost the same line of action they could be combined into a lumped muscle

- This combination of muscles contribute most to the joint moments based on their PCSA [56]
- The line of actions lies for more that 90% in the sagital plane
- These muscle are used in other models that have a walking movement

The biggest problem expected were the biarticular muscle. Therefore the possible extra monoarticular muscle that could be added/replacements:

- Biceps Femoris short head
- Gluteus Maximus
- Iliopsoas[2] (Lumped muscle of Iliacus and Psoas)

In figure 4.1 on page 29 the position of the different muscles are available

4.2 Software choices

The models in this project are made with computer programs. The choice for these programs is made before the start of the actual project (SimMechanics) by the supervisors or it was the easiest program to use for the inverse dynamics on muscle activated models (Anybody).

4.2.1 SimMechanics

SimMechanics allows engineers to model and simulate mechanical systems in the Simulink environment. With SimMechanics, you can directly model mechanical components (bodies and joints), simulate their motion, and analyze the results without having to derive the mathematical equations governing the system.

Technically, the system is characterized by the following properties:

- Models and simulates rigid body mechanical systems within Simulink.
- Provides full modelling hierarchy allowing mechanical blocks to be grouped with other block types.
- Uses Simulink's solvers for accurate three-dimensional analysis and simulation Contains comprehensive joint and constraint libraries.
- Models linear and angular motions, forces, and torques.
- Provides trimming and linearization capabilities for control system design.
- Enables visualization and animation of mechanical systems using either Virtual Reality Toolbox or MATLAB graphics (Handle Graphicső).
- Performs kinematic, forward, and inverse dynamic analysis of mechanical systems.
- Uses O(n) recursive algorithms to solve equations of motion for multibody systems.

[2] If muscles had the same function and almost the same line of action they could be combined into a lumped muscle

- Provides multiple local coordinate systems for model definition.
- Ability to generate stand-alone C code using Real-Time Workshop.

For above and more information see the website [3].

In this project SimMechanics 1.0 is used. Also a network version 1.1 was available, but this version is only used for large calculations because of its unstable behavior. With the newest Matlab (release 13) an updated SimMechanics 2.0 is available with new features.

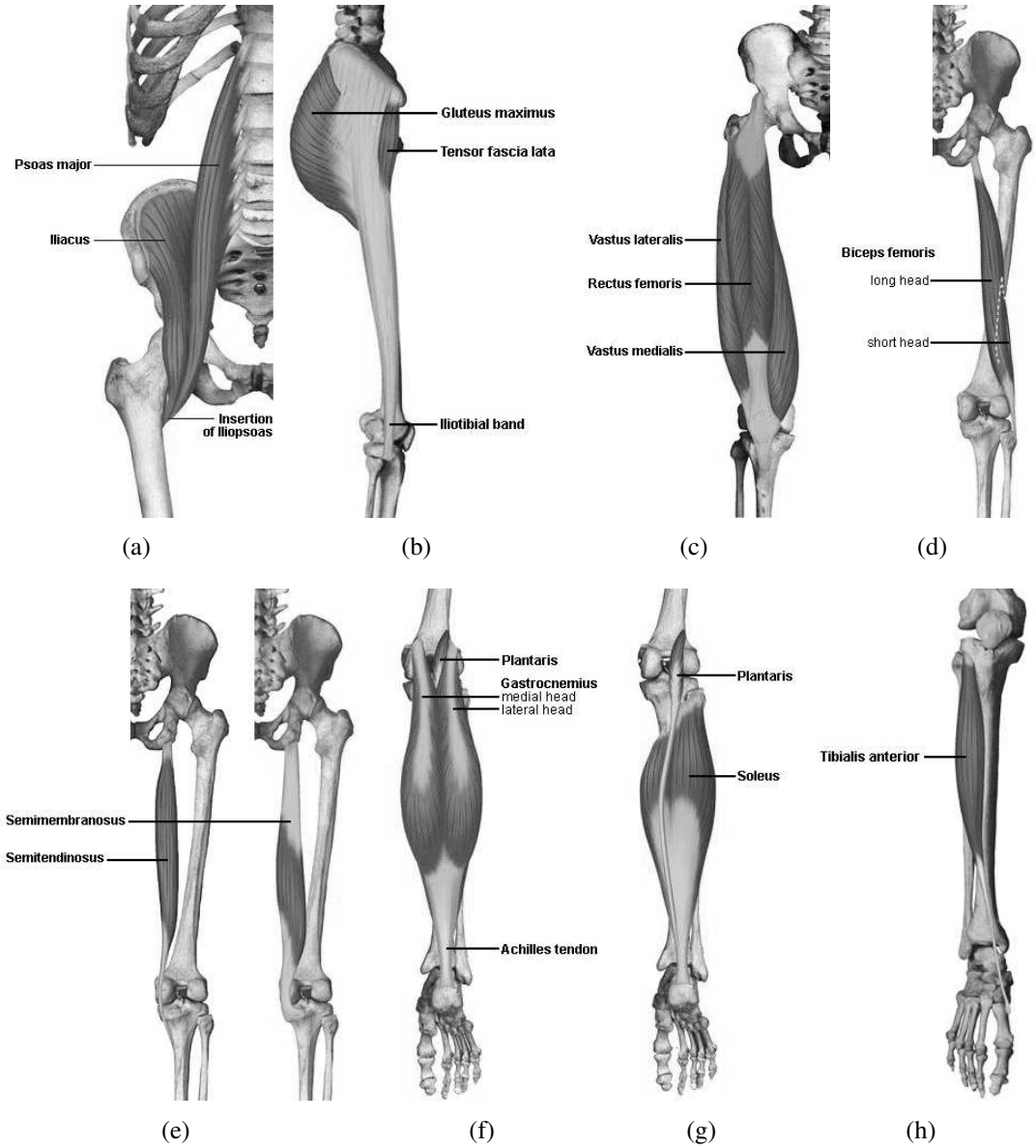

Figure 4.1: *Overview of muscles used in this project. (a),(c),(h) are postior view. (d),(e),(f),(g) are anterior view. (b) is seen from sagital plane. From* http://eduserv.hscer.washington.edu/hubio553/atlas.

4.2.2 Anybody

The AnyBody Modeling System is a software system for simulation of human movement. It can model smaller or larger subsets of the musculo-skeletal system and compute muscle forces, joint reactions, metabolism, mechanical work, efficiency, etc. for given movements.

Technically, the system is characterized by the following properties:

- It uses an optimization technique to solve the muscle recruitment problem and reverses this by means of other optimization techniques so that forward dynamics problems can also be treated.
- It handles static and dynamic models Models are fully three-dimensional.
- It runs on the MS Windows platform.
- It handles very large models on small computers.
- It is entirely feasible to analyze a model with several hundreds of muscles on an ordinary PC.
- Models are developed in the body modelling language AnyScript.

AnyBody is currently in its alpha testing phase. For above and more information see the website [2].

In this project the installation version 0.0.2 alpha is used and updated with a 0.0.3 alpha exe-file with a improved interpol driver. For future projects: It was was not an official release, so ask Mark de Zee or John Rasmussen to get the correct version of Anybody with the improved selectable (Bezier or PiecewiseLinear) interpol driver.

4.3 Data-sets

The complete biomechanical model will need a certain amount of parameter settings, input data and verification data. A lot of data is available in the biomechanical area, but this data is not always suitable. The main problem is the huge amount of possible options for the different data-sets with all their own advantages and disadvantages. Another problem is the variation in data-sets, because a difference in personal characteristics and measuring conditions. In this section the possible options for the different groups of data-sets are discussed.

4.3.1 Joint angle

This part of the data-set is a widely described in many articles and books, but the greatest part is given via a a graph with margin bands. A few number of RAW-data-set have been found on the internet [1]. These digital sets are the digital versions of the data used by Winter [56] and Vaughan et. al [15]. The major reason for not using this data was:

- Both data-sets only have ± 60 samples/cycle

- No information about EMG measured at the same persons at the same time
- The data of Winter is not an average of several steps

Many data-sets at the SMI are only containing the ankle and sometimes the knee angle, together with EMG signals of some muscles. Erika Spauch collected useable joint angular data during walking together with EMG of the same person at the same experiment. Characteristics of the data:

- The data is collected at a sample frequency of 2kHz
- The data is averaged over 28 cycles
- The angle data is collected with 3 angular sensors on the right hip, knee and ankle.
- The walking speed was approximately 3 km/h
- The data is collected on a treadmill at SMI

The only problem with the data was an unknown offset and a very high knee flexion of 90 degrees. The next steps were performed to get the angle data of figure 4.2:

- The angle data is re-sampled to get equal number of samples/cycle for all the 28 cycles.
- The 28 cycles are averaged.
- The knee angle is restricted to a minimum of 0 degrees flexion (this criteria determines the knee offset).
- The knee angle is multiplied with a constant to set a maximum knee flexion to a normal knee angle-curve with a maximum of 70 degrees.
- The hip angle range (22.5 degrees) was very small compared to other known hip angle-curves and is doubled to 43 degrees (this and previous step changed the walking speed).
- The offset of the hip and ankle were adjusted so the left toe had contract with the ground at the time of right heel contact.
- The angle data is filtered with a moving average to prevent high frequent velocity curves.
- The velocity is calculated numerical for every angle sample.
- The previous steps is performed on the velocity to get the acceleration.
- The angle,velocity and acceleration for the left leg are shifted in time (1/2 cycle time).

4.3.2 EMG

The same problem mentioned finding the angle-data is finding the useful EMG-data, though many people did measurements on part of the lower leg muscles. Almost nobody recorded a wide range of muscles on many subjects, which results in an average EMG-pattern. The best option was to use the EMG-data recorded with the angle data of Spauch, so there is a certain correlation between the two sets. But her measurements contained only the EMG of a few lower leg muscles.

A useful dataset is a set of Hof et al. [22], which is available on the internet. They recorded the EMG 14 lower leg muscles:

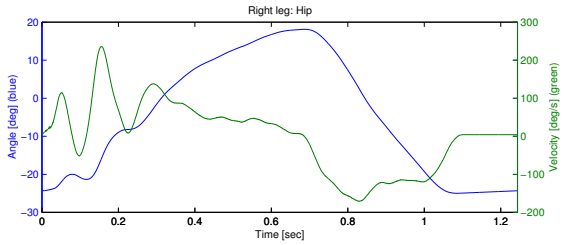

(a) Hip

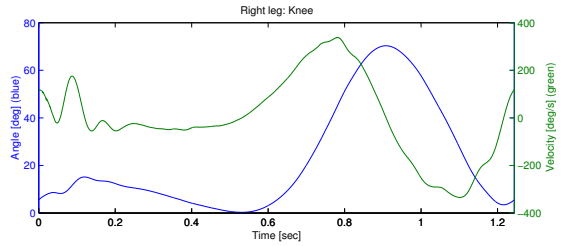

(b) Knee

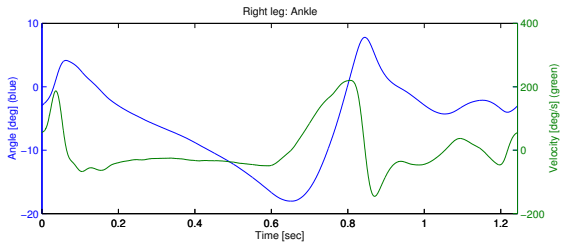

(c) Ankle

Figure 4.2: *Data of Spauch after processing (Angle = blue and angle velocity = green)*

1 Soleus	8 Rectus Femoris
2 Gastrocnemius Medialis	9 Biceps Femoris Long Head
3 Gastrocnemius Lateralis	10 Semitendinosus
4 Peroneus Longus	11 Semimembranosus
5 Tibialis Anterior	12 Gluteus Maximus
6 Vastus Medialis	13 Gluteus Medius
7 Vastus Lateralis	14 Adductor Magnus

The data is an average of 10 different subjects. There are even 5 different sets collected at different speeds ranging from 0.75 - 1.75 m/s. An import conclusion of Hof et al. could be useful in future projects, because they showed a linear-biased relationship between speed and EMG pattern. With a complete working model an easy adjustment in the speed-constant should result in the correct neural input.

Though Hof et al. did not record the joint angles during walking the EMG-data was the best available. To check if the data is usable in combination with the angle data of Spauch, the EMG-patterns of the Soleus (see figure 4.3), Vastus Lateralis, Tibialis Anterior and Rectus Femoris are compared. Part of this comparison is available in figure 4.3 and the rest of the figures is printed in Appendix A (figure A.2 - A.5). In all figures the amplitude and shape

are comparable, especially the on and off-set of the curves. This is the reason to conclude that Spauch's measurement is correlated with Hof's data, so the angle data of Spauch can be combined with the EMG of Hof et al.

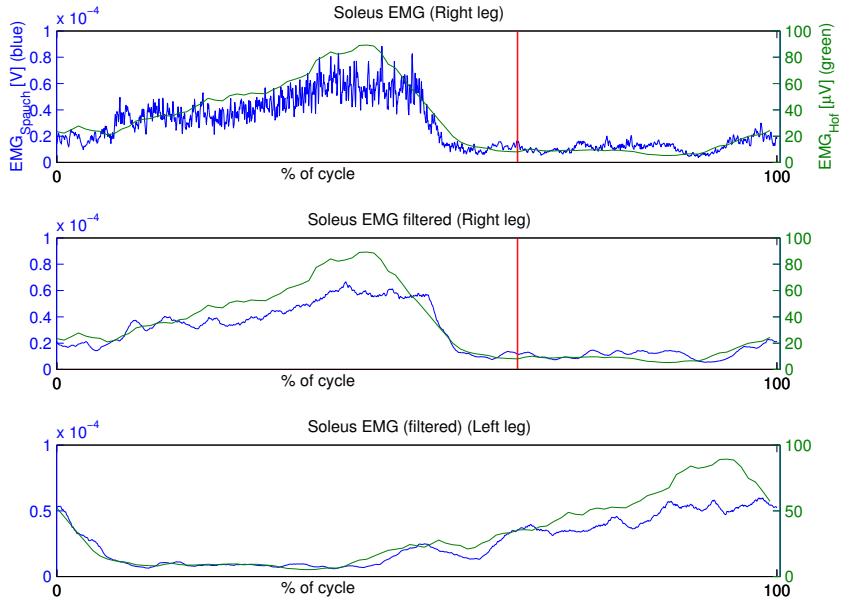

Figure 4.3: *Soleus EMG-data measured by Spauch (blue) and Hof et al. (green) compared. The data of Spauch was of the left and right leg and Hof et al. of one unspecified leg. The red line is start of the swing-phase (65% for a speed of 0.75 m/s as given by Hof et. al [22])*

4.3.3 Muscle force

To evaluate a muscle model not only a EMG or neural-input is necessary, but also a measured tendon force. In contradiction to the project of Huber [26], where a muscle model activated by FES, the forces can not be calculated from joint moments. The use of joint moment to calculate 1 specific tendon force is too dangerous, because the synergistic muscle also can produce force/moment and also extra antagonistic force/moment is not taken into account.

Therefore a force measured on the tendon is the only possible option, and of course the best data is measured during walking. Though measuring tendon force in human is difficult, it is possible with an optical measurement device. Not published data measured by Masaki Ishikawa at the Neuromuscular Research Center, Department of Biology of Physical Activity at the University of Jyvaskyla was available. Four different data-set were received with EMG of the Soleus, Gastrocnemius, Tibialis Anterior, Rectus Femoris, Vastus Medialis, Vastus Lateralis, Biceps Femoris. The ground force reaction of both feet in x and y direction and an optical signal to calculate the Achilles tendon force.

Though all the EMG of this data-set could be used, the number of unknown conditions were too high and it was the EMG of 1 person with not always normal walking conditions. After processing the RAW-EMG of the soleus and gastrocnemius is used to verify the muscle model (see figure 4.4 for the 4 data-sets after processing).

The 4 data-sets, with the different conditions

1. Bjorn_3: Normal walking
2. Bjorn_4: Normal walking
3. Bjorn_5: Walking on a soft surface
4. Bjorn_6: Ramp walking

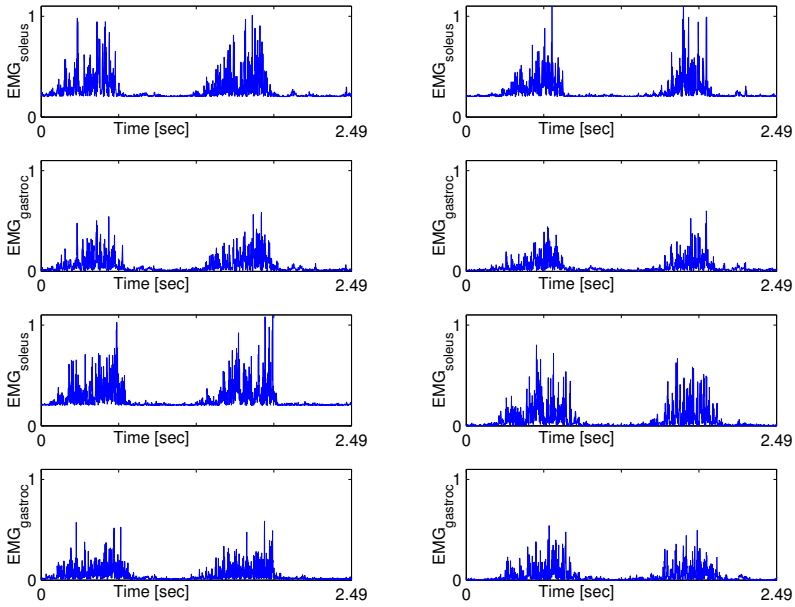

Figure 4.4: *The processed RAW-EMG measured by Ishikawa used to verify the muscle model*

4.3.4 Muscle anthropometry

When a muscle model is build and used with a model of the skeletal system, like in this project the parameters of the muscle have to be chosen carefully. The largest and suitable data-set was found on the internet [1]. This complete description of the data-set is used by Delp et al. [16] and presents the following data (available in Appendix C):

- Origin and insertion points the muscle/tendon
- Maximum isotonic force at optimal length (calculated with eq. 3.6)
- Optimal fiber length (= L_o)
- Tendon slack length (= T_s)
- Pennation angle (= α)
- Muscle function

As already mentioned in section 4.1 some of the chosen muscle can be combined into a lumped muscle. To get the correct values for the lumped muscle the idea was to use the PCSA as a weight-factor. Because the only Fmax is available and linear to the PCSA the Fmax is usuable as a weight-factor (see eq. 4.3)

Transformation	X	Y	Z
Pelvis -> Hip	$+0.0707$	$+0.0661$	-0.0835
Femur -> Hip[3]	$=$	$\cdot 0.46/0.401$	$=$
Tibia -> Knee	$=$	$=$	$=$
Patella -> Knee	$+0.0444$	-0.02153	-0.0024
Calcn -> Ankle	-0.04877	-0.04195	$+0.00795$

Table 4.1: Transformations for the co odinates from Delps model to model of this project

For example the gastrocnemius uses the next equations. With and index of 1 and 2 for the muscles and index 3 is for lumped.

$$F_{max_3} = F_{max_1} + F_{max_2} \tag{4.1}$$

$$Penn_3 = \frac{Penn_1 \cdot F_{max_1} + Penn_2 \cdot F_{max_2}}{F_{max_3}} \tag{4.2}$$

$$L_{o_3} = \frac{L_{o_1} \cdot F_{max_1} + L_{o_2} \cdot F_{max_2}}{F_{max_3}} \tag{4.3}$$

4.3.5 Muscle connection points

Though the data-set of Delp has a complete set of muscle connection points, the use of these points can not be used immediately, because the data-set is based on a specific person with specific bone dimensions and positions of specific markers. To transfer the point to the right points in this project model directions the transformations in table 4.1 are performed (based on a comparison between both models). For the lumped muscles the same averaging is performed for the connection points as like for the optimal fiber length (see eq. 4.3)

Though the origin and insertion points appeared not fully correct, the completeness of the data was a suitable starting point. In the middle of this project an evaluation of the muscle moment arms is performed. This is discussed in section 4.4.3 on page 41 and seemed to play an important role with determining the muscle force needed for a certain movement.

4.3.6 Determination of muscle tendon length

The last unset parameter is the tendon length. In the set of Delp the Tendon slack length is given. This parameter is not useful, because all the connection points are changed, bones have different lengths and an other parameter is needed for the muscle model. The parameter needed for the muscle model is the tendon length at maximum muscle contraction at optimal length. The length can be measured if the joint angle is known for the specific point. In the table 4.2 the intentional 6 muscles are shown. This data is obtained from an internal report by Mark de Zee for an Anybody model.

[3]Because the thigh-bone was different in length and the connection-point were far from the hip. Not necessary for the knee, because connection points closer to the knee.

Muscle	Ankle joint angle	Knee joint angle	Hip joint angle
Soleus	-15		
Tibialis Anterior	20		
Gastrocnemius	-15	0	
Vastus Lateralis		70	
Rectus femoris		70	0
Hamstrings		0	-50

Table 4.2: Overview of joint positions where the muscle fibre has its optimal length. Ankle joint: 0 deg is neutral position, positive is plantar flexion, negative dorsi flexion. Knee joint: 0 deg is straight knee, positive is knee flexion. Hip joint: 0 deg is straight hip, negative is hip flexion.

Remarks and references:

1. Soleus (Maganaris [34]).
2. Tibialis Anterior (Maganaris [34]; Marsh et al. [36]). Maganaris finds 30 and Marsh et al. finds 10 $\Rightarrow$ average 20.
3. Gastrocnemius (Herzog et al. [20]; Cresswell et al. [14]; Hoy et al. [25]; Sale et al. [49]). The mentioned references all find that the gastrocnemius works on the ascending limb. That's why it might be reasonable to choose the same ankle angle as the soleus and the knee totally extended.
4. Vastus lateralis (Ichinose et al. [29]). Might be reasonable to use this value for all the vasti muscles.
5. Rectus femoris. Hoy et al. (Hoy et al. [25]) found with modelling a knee joint angle of 50 deg together with a hip joint angle of 60 deg. This, however, didn't work too well in the cycle model made by the group of Anybody. That's why the value has changed to the same as vastus lateralis (70 deg knee angle with extended hip).
6. Hamstrings (Hoy et al. [25]).

4.4 Mechanical model

In this section the implementation of the mechanical model is explained. In the beginning of the project it seems the mechanical model of Huber [26] was correct, but the same verification as explained in the next section brought a wrong implementation of the SimMechanics muscle to light. This is possibly the origin of his not successful mechanical verification.

4.4.1 Skeleton

The skeleton of the human lower leg is constructed completely with the used of SimMechanics. The complete layout of this model is not printed out, but can be viewed on the CD-Rom which is made with this report. A schematic view of the model is visible in figure 4.5. The 7 segments: HAT, Thigh (2x), Shank (2x) and Foot (2x) are modelled with the formulas form Vaughan et al. [15]. The kneecap is modelled like a massless segment that rotates at a certain distance around the knee and the kneecap tendon is a line with a fixed length (see figure 4.6).

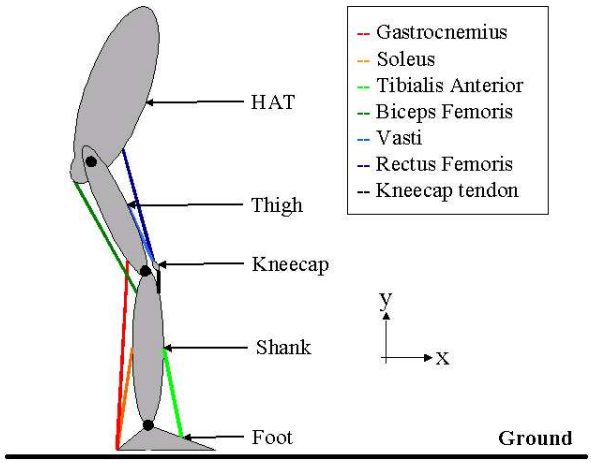

Figure 4.5: *A simple schematic view of segments and muscles*

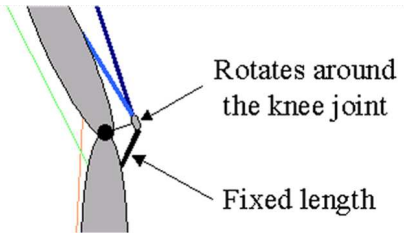

Figure 4.6: *A simple schematic view of kneecap system*

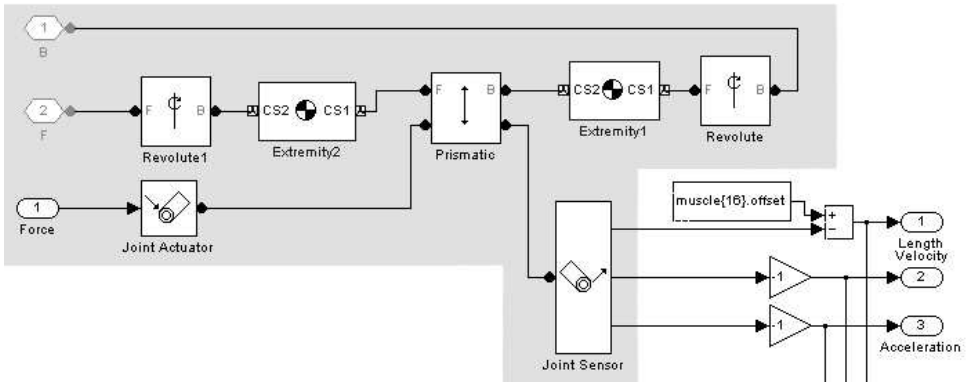

Figure 4.7: *Muscle/tendon block in SimMechanics. The grey area contains the specific SimMechanics blocks. The "Force Element" is the actual muscle/tendon-unit. It is modelled as a prismatic joint between the origin and insertion points (= muscle line of action). The prismatic joint is activate by a force equal to the F_{tendon} and the joint sensor gives direct information about the muscle length, velocity and acceleration. The 2 revolute joints are necessary to give the muscle rotational free movement and the 2 extremities are bodies of 1 gram and no size, necessary to connect 2 joints.*

4.4.2 Mechanical muscle

SimMechanics is not specific build to model a biomechanical model, but in the previous project of Huber [26] tested several muscle models. His suggestion appeared to not correct and much too complicated, therefore a special new muscle/tendonblock is build and tested.

During this project only a straight line muscle is completely tested. A few attempts of muscles with wrapping points (like SIMM) or via-point (like Anybody) did not perform as intended.

Because SimMechanics calculate the necessary mathematical equation internal you are never sure if the model is behaving as intended. A test-system like in figure 4.8 is build and 2 tests are performed to verify the model of figure 4.7.

1. Verify the moment arm and sensor output of the muscle
2. Apply a force to the prismatic joint and verify the length of the muscle

Moment arm

The muscle of the system in figure 4.8 is build in SimMechanics. First the moment arm r is calculated with the equations:

$$i = \cos(\alpha) \cdot Y \tag{4.4}$$

$$j = X - \sin(\alpha) \cdot Y \tag{4.5}$$

$$\beta = \arctan(\frac{i}{j}) \tag{4.6}$$

$$r = \sin(\beta) \cdot X \tag{4.7}$$

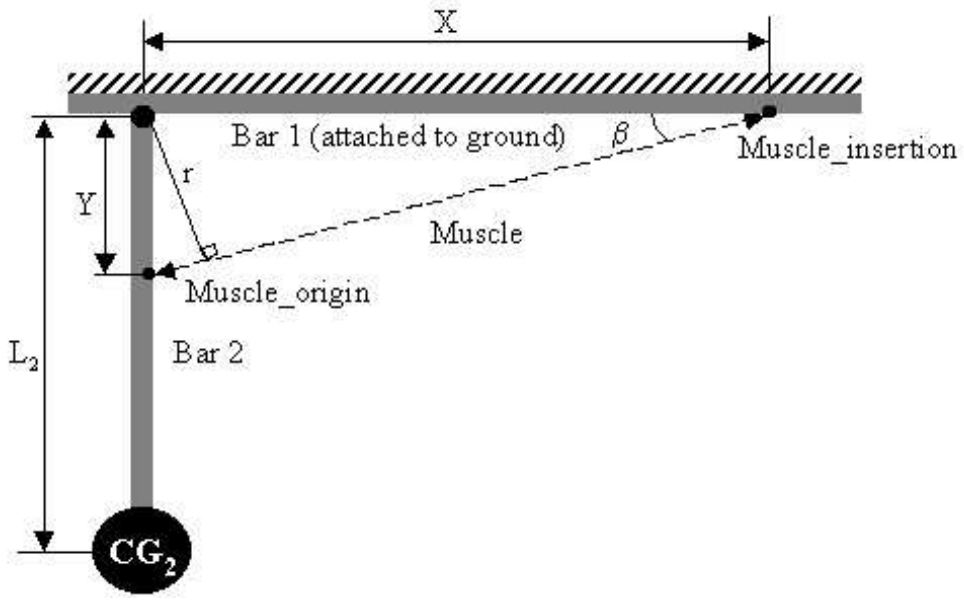

Figure 4.8: *Schematic view of muscle test system*

Another option is to calculate the moment arms is by the force produced by a muscle F_m over a very small tendon excursion dL, that equals the work done by a moment M about the axis of movement through and angle d_{theta} which is infinitesimally small. This is exactly the formulas needed to simulate the moment arm in SimMechanics.

$$F_m \cdot \partial L_{muscle} = M \partial \alpha \tag{4.8}$$

The moment arm then is defined by:

$$r = \frac{M}{F_m} = \frac{\partial L_{muscle}}{\partial \alpha} \tag{4.9}$$

Muscle force

To test the muscle, different output the equilibrium forces are calculated and compared with the simulation results where a muscle force is given and the alpha is the output.

To calculate the necessary muscle force there needs to be a equilibrium in forces and moments. For the muscle force:

$$\begin{aligned} \sum M_b &= 0 \\ L_2 \cdot F_{z_{rot}} - Y \cdot F_{m_{rot}} &= 0 \\ L_2 \cdot F_z \cdot \sin(\alpha) - Y \cdot F_m \cdot \cos(\gamma) &= 0 \\ F_m &= \frac{L_2 \cdot F_z \cdot \sin(\alpha)}{Y \cdot \cos(\gamma)} \end{aligned} \tag{4.10}$$

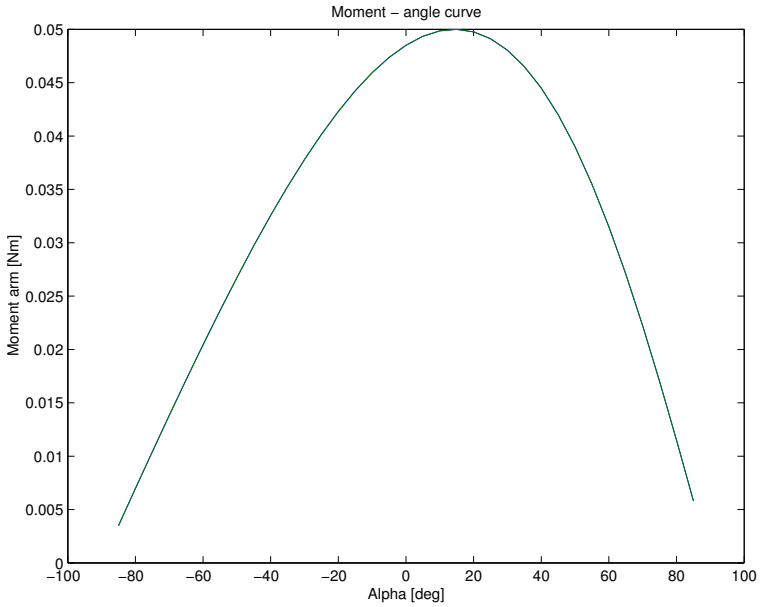

Figure 4.9: *Example of moment curve of the test system of figure 4.8 The comparison between the simulated 4.9 and calculated 4.7 curve resulted in an* $error < 10^{-9}$ *and an* $error_{rel} < 10^{-9}$ *for different lengths in (X,Y and L2). These errors are so small that there are neglectible and only have their origin in the numerical calculation. The eq. 4.9 is later used to calculate the moment arms of the different muscles to verify the muscle connection points.*

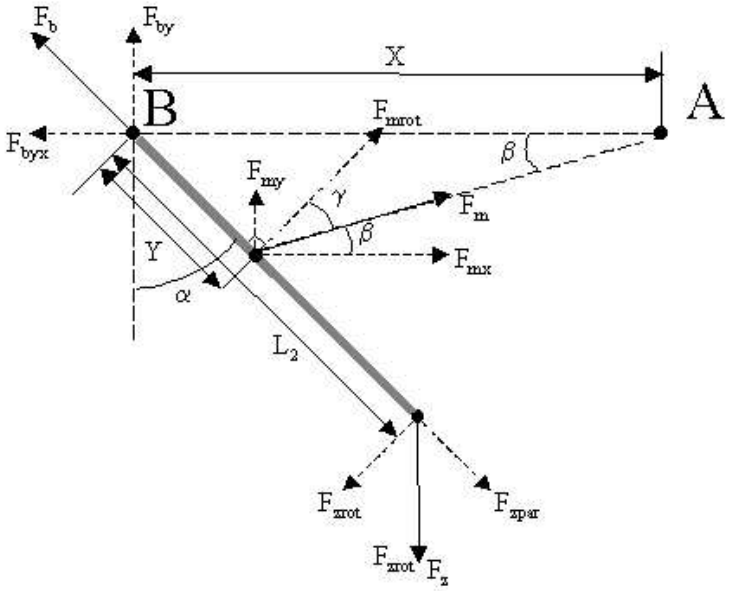

Figure 4.10: *Schematic view of the forces in the muscle test system* $\gamma = \alpha - \beta$

And to verify all the force in the system the force at rotational point B is calculated.

$$\sum F = 0$$

$$\sum F_x = 0, \qquad \sum F_y = 0$$

$$F_{m_x} - F_{b_x} = 0, \qquad F_z - F_{m_y} - F_{b_y} = 0$$

$$F_{b_x} = F_m \cdot \cos(\beta), \qquad F_{b_y} = F_z - F_m \cdot \sin(\beta)$$

$$F_b = \sqrt{F_{b_x}^2 + F_{b_y}^2} \tag{4.11}$$

The comparison between the simulated and calculated force resulted in an $error < 10^{-1}$ and an $error_{rel} < 10^{-3}$ These errors are so small that there are neglectible and only have their origin in the numerical calculation. The muscle/tendon block of figure 4.7 is therefore implemented for all the muscles

4.4.3 Muscle moment arm verification

Though the measurements of Delps muscle are measured on a correct way, when they are implemented in the mechanical model the moment arms do not agree with the values given in the literature. A part of this difference could be the modelling the muscle like a straight line. A verification of the moment arm is performed with the values given in the literature with the following references.

1. Tibialis Anterior (Maganaris [33])
2. Soleus and Gastrocnemius (ankle) (Maganaris et al. [35])
3. Gastrocnemius (knee), Vastus and Rectus Femoris (Buford et al. [10], together with information from the Anybody group)
4. Hamstrings (Herzog and Read [19])

In Appendix C all the exact used values are listed. This includes the original points from Delp, the adjusted point and the points after moment arm verification.

In figure 4.11 - 4.13 on page 42 - 43 the moment arms for the different muscles are shown. Not only a clear difference between the Delp en verification line is visible but also the reason for the so called Lombards paradox.

The Lombard's paradox is know as co-activation of hamstrings and rectus femoris (two antagonistic muscles) during the activity of standing from a sitting position. The reason for the standing despite the co-activation of the two antagonistic movement is due to the difference in moment arms at either the hip or the knee. The moment arm for the rectus femoris is greater at the knee in the sitting position and the difference is even bigger at standing. And the moment arm of the hamstring is bigger at the hip. A co-activation of the muscles will therefore result in knee and hip extension, which is know a standing from a sitting position.

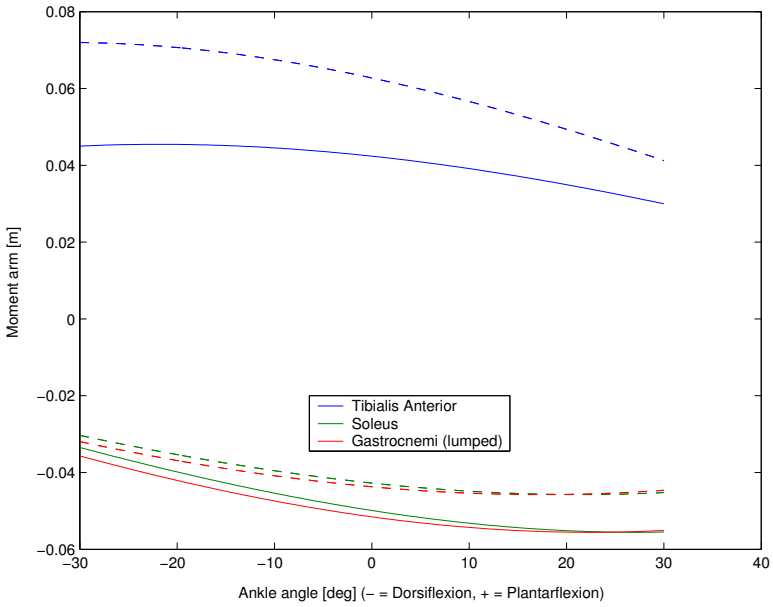

Figure 4.11: *Moment arms for muscles around the ankle joint (Solid line: verified, dashed line: Delp)*

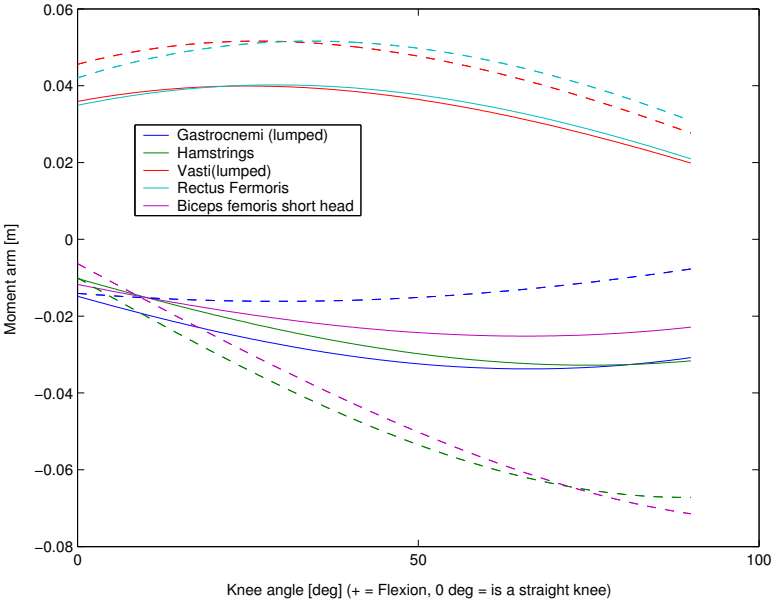

Figure 4.12: *Moment arms for muscles around the knee joint (Solid line: verified, dashed line: Delp)*

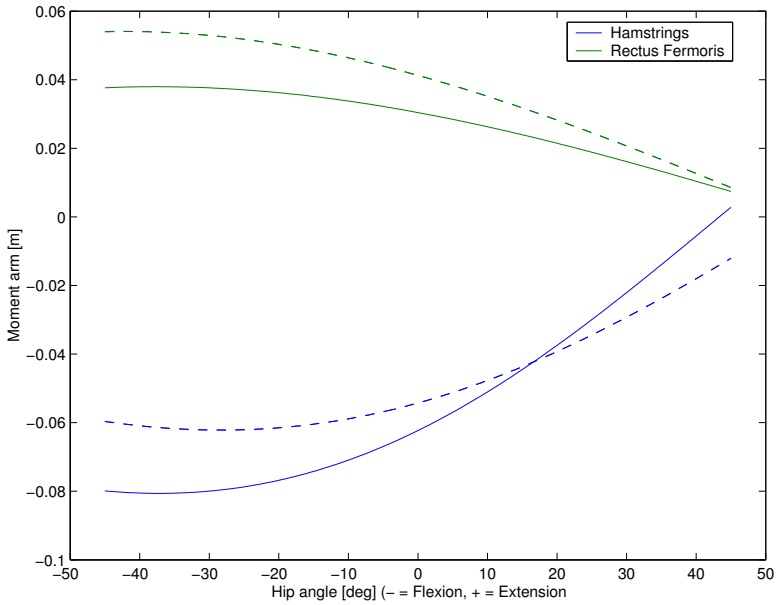

Figure 4.13: *Moment arms for muscles around the hip joint (Solid line: verified, dashed line: Delp)*

4.5 Muscle model

After the construction of the correct mechanical model of the muscle the neural part of the muscle is implemented. Although the first idea was to find a force-pattern without a muscle model, this was to hard. More about that part in the results chapter. In section 3.2 different options for a muscle model are discussed. Because a simple model based on 2nd-order filter was not successfull the best option was to implement the muscle model of Cheng et al. [12]. This model is schematic given in figure 4.14 on page 44. Although it has a lot of individual blocks it is able to describe the individual characteristics of a muscle very good.

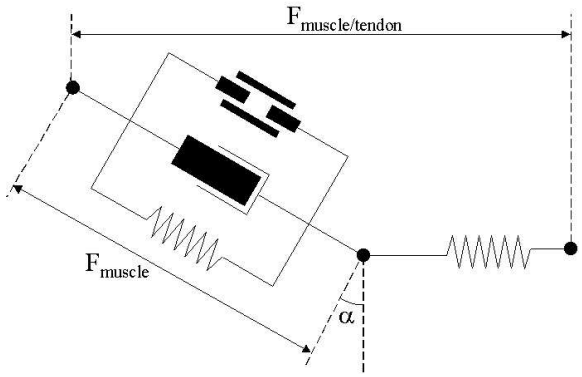

Figure 4.14: *Basic muscle model of figure 3.5 with the implementation of the pennation angle α as mention in section 2.2.1 and figure 2.2 on page 7*

The blocks in figure 4.14 are implemented with a number of equations (eq. 4.12-4.21). These equations are found with curve fitting from cat muscles. Cheng et al. extrapolated the parameters of the function to characteristic human muscle fibers. They implemented this system in a model called "Virtual Muscle". In the virtual muscle there is an distinction between fast and slow fibers. In the future this is also a good option for the human locomotion model, but for this project all the parameters are based on an average of 10% super slow, 40% slow fibers and 50% fast fibers. The values for this parameters are listed in Appendix B

$$F_{SE}(L^T) = c^T k^T \ln\left\{\exp\left[\frac{(L^T - L_r^T)}{k^T}\right] + 1\right\} \tag{4.12}$$

$$F_{PE1}(L) = c_1 k_1 \ln\left\{\exp\left[\frac{(L/L_m ax - L_{r1})}{k_1}\right] + 1\right\} + \eta V \tag{4.13}$$

$$FL(L) = \exp\left(-\left|\frac{L^\beta - 1}{\omega}\right|^\rho\right) \tag{4.14}$$

$$FV(V, L) = \begin{cases} (V_{max} - V)/(V_{max} \pm (c_{v0} + c_{v1}L)V), & V \leq 0 \\ (b_v - (av0 + av1L + av2L^2)V)/(b_v + V), & V > 0 \end{cases} \tag{4.15}$$

$$\dot{L}_{eff}(t) = \frac{(L(t) - L_{eff}(t))^3}{T_L(1 - A_f)} \tag{4.16}$$

$$n_f(L_{eff} = n_{f0} + n_{f1}\left(\frac{1}{L_{eff}} - 1\right) \tag{4.17}$$

$$T_f(Af, L) = \begin{cases} T_{f1}L^2 + T_{f2}f_{env}(t), & \dot{f}_{eff}(t) \geq 0 \\ (T_{f3} + T_{f4}Af)/L, & \dot{f}_{eff}(t) < 0 \end{cases} \tag{4.18}$$

$$\dot{f}_{int}(t, f_{env}, T_f) = \frac{f_{env} - f_{int}}{T_f} \tag{4.19}$$

$$\dot{f}_{eff}(t, f_{int}, T_f) = \frac{f_{inf} - f_{eff}}{T_f} \tag{4.20}$$

$$Af(f_{eff}, n_f) = 1 - \exp\left[-\left(\frac{f_{eff}}{a_f n_f}\right)^{n_f}\right] \tag{4.21}$$

The equations 4.22-4.25 are not used, but could be added to ge a better and more accurate model. In the virtual muscle these extra effects are implemented, but have only a minor effect. To keep the muscle model simple in this project these equations are not implemented.

$$F_{PE2}(L) = c_1 k_1 \ln\left\{\exp\left[\frac{(L/L_m ax - L_{r1})}{k_1}\right] + 1\right\} + \eta V \tag{4.22}$$

$$\dot{S}(t, f_e ff) = \frac{a_s - S(t)}{T_s}, \qquad a_s = \begin{cases} a_{S1}, & f_{eff}(t) < 0 \\ a_{S2}, & f_{eff}(t) \geq 0 \end{cases} \tag{4.23}$$

$$\dot{Y}(t) = \frac{1 - c_y[1 - exp(-|V|/V_Y)] - Y(t)}{T_Y} \tag{4.24}$$

$$Af(f_{eff}, n_f, Y, S) = 1 - \exp\left[-\left(\frac{YSf_{eff}}{a_f n_f}\right)^{n_f}\right] \tag{4.25}$$

The equations 4.12-4.21 are implemented in schematic figure 4.15. To get a quick view of the equations, the plots in figure 4.16 and 4.17 should be enough. In the upmost plots of figure 4.16 also the curve of the slow and fast fibers of Cheng et al. are drawn.

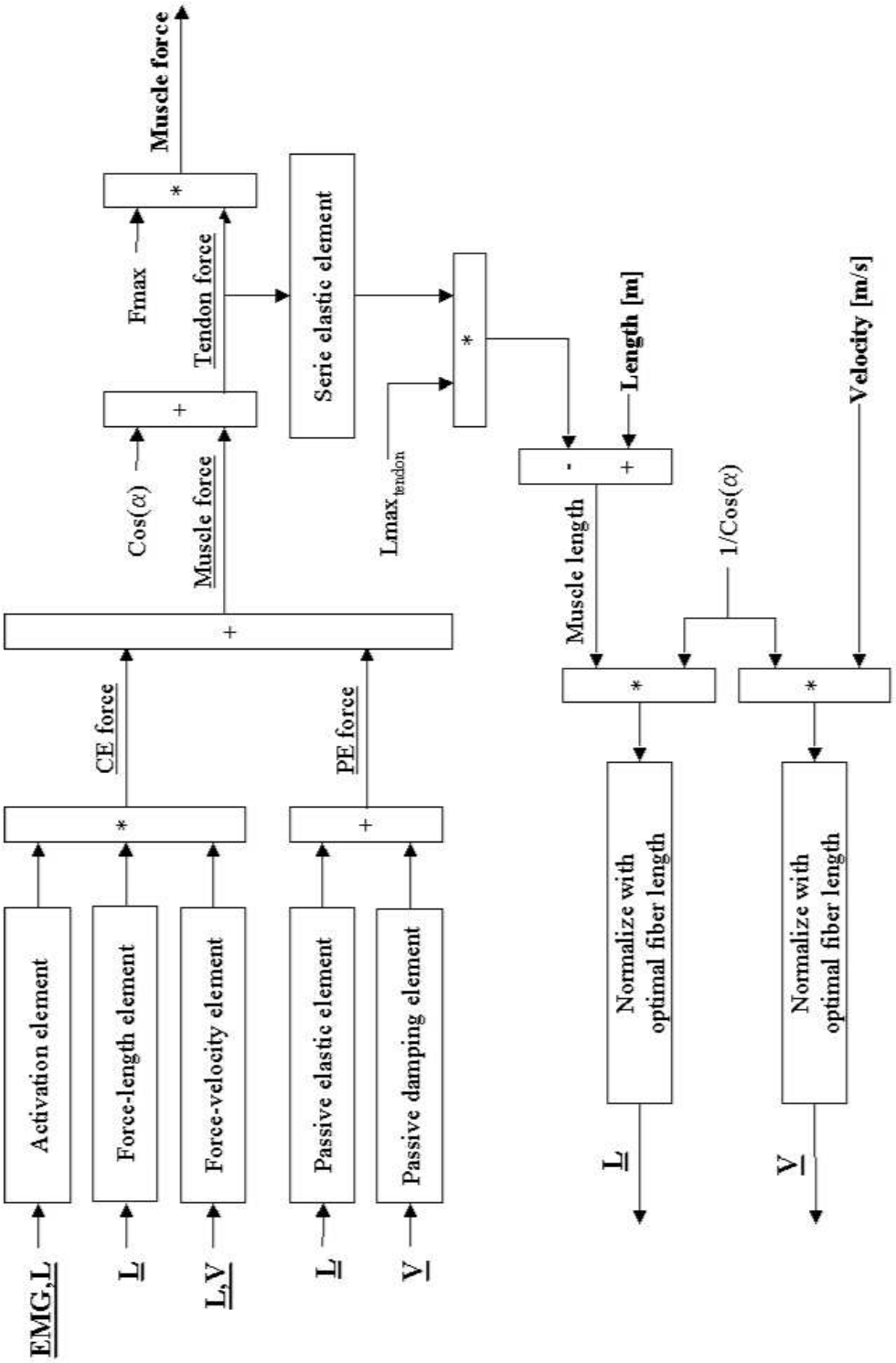

Figure 4.15: *The schematic implementation of the muscle*

4.6 Ground contact

Implementation of the ground contact is also tested. The implementation was the same as in figure 3.2 on page 16. When the mechanical skeleton is activated with joint angles this

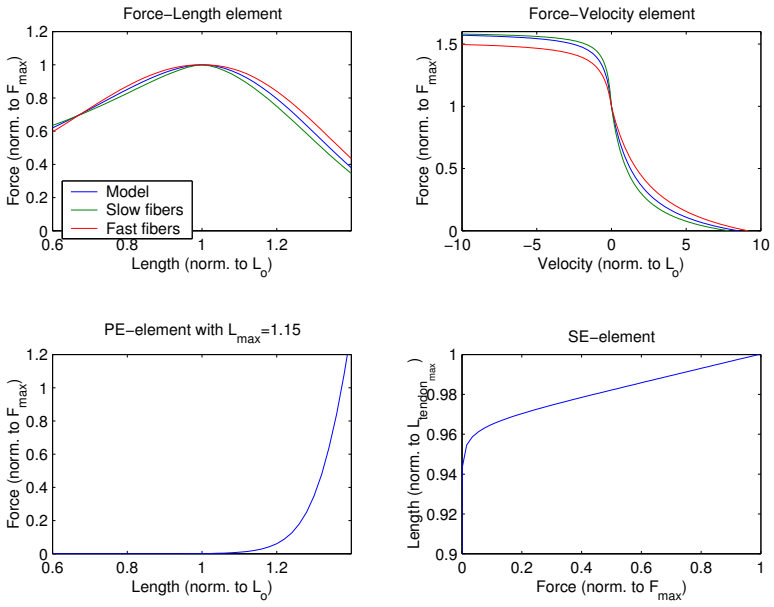

Figure 4.16: *The curves of the passive parts (eq. 4.12-4.15)*

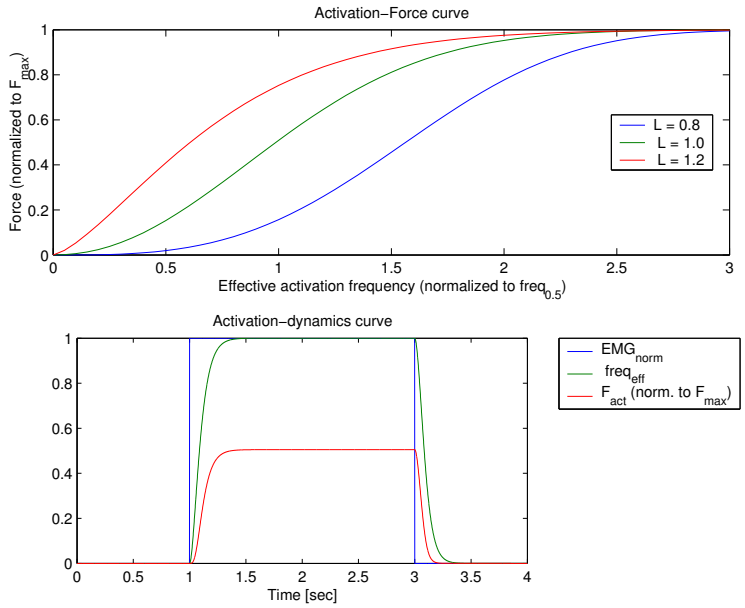

Figure 4.17: *The curves of the activation dynamics (eq. 4.16-4.21)*

implementation is very successful. But when every joint is moment activated or if the model is muscle activated this implementation slows down the whole system. The reason is a high frequent feedback of the damper. Because the damper coefficient has to be very high small speed changes gave a high change in damper feedback, which was high frequent. A solution where this feedback was implemented with a low-pass filter the results where getting better, but because at that time the needed muscle forces where unknown the implementation is not finished for this part of the model.

CHAPTER 5

Results

5.1 Muscle model verification

The muscle model in section 4.5 is verified with a specific fast human muscle (Claudius femoris) by the developers of the model (Alfred E. Mann Institute for Biomedical Engineering, USA). For the use of this model Cheng et al. [12] recommend a linear relation between EMG and activation of a 1 muscle model with 1 motor unit. The expectation is that the muscle can predict the muscle force based on EMG-input, because EMG is equal to the frequency information, which is the required input of the model. As mentioned before the force data was not present as an individual input output data, but the combined force of the GAS and SOL. Though these muscle have not the exact same characteristics the test is performed with the average motor unit to see if the model can be used.

The verification is not perfect, because the used data (muscle model, EMG, anthropometry, muscle length) are based on different measurements on different persons and with different conditions. For both muscles all the parameters are fixed (as given in table B.1 (muscle model) and table C.1 and C.4 (muscle connection points/lenght)), except the scaling factor of the EMG input. This parameter is adjustable because it is not measured. The expectation was that a specific combinations of the 2 scaling factors result in the right tendon force curve of the Achilles tendon. *!!Note: The EMG-signal is multiplied with the scaling factors instead of divided which is normally performed with an normalization factor.*

A simple test resulted in a range for both scaling factors (0-5.9 for soleus and 0-24.9 for gastrocnemius). With a step of 0.1 in the scaling factor this results in 60*250 =15.000 possible combinations. A second test calculated the possible tendon forces by adding the 2 predicted muscle forces together. The values of the scaling factors are evaluated with 6 different cost functions (see figure 5.1). These cost functions are based on the const functions used in other

prediction models and specialized to this specific model.

1. Mean of the error curve[1] *(Linear-criterium)*
2. Mean of the absolute error curve *(Absolute-criterium)*
3. Mean of the squared error curve *(Squared-criterium)*
4. Every data-point is checked. If the error is in the band [-25 N, 25 N], this data-point was ok. If no, the cost-value is increased with the $\mid error \mid -25N$ *(Band-criterium)*
5. Every data-point is checked. If the error is in the band [-25 N, 25 N], this data-point was ok. If no, the cost-value is increased with 1. The cost value/# data-points will give a percentage of data-points not close enough to the measured force *(Simple Band-criterium)*
6. Every data-point is checked. If in error is in band [-25 N, 25 N] compared to measured data 10 ms around the data-point, this data-point was ok. If no, the cost value is increased with 1. The cost value/# data-points will give a percentage of data-points not close enough to the measured force *(Simple area-criterium)*

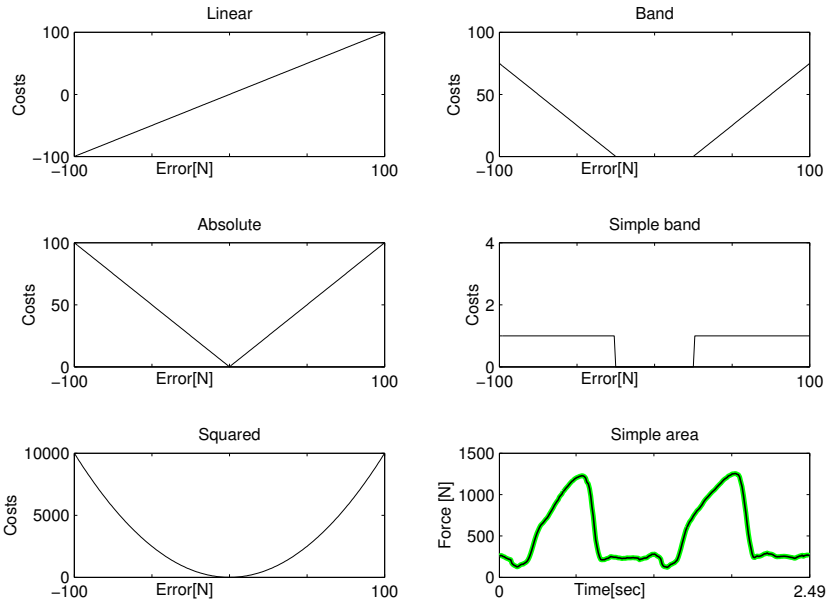

Figure 5.1: *The 6 listed cost-functions. For the simple area-graph a data-point outside the green area will increase the cost value with 1.*

The cost-functions give an idea of the quality of the estimated force-curves. It appears that a (large) range (of the total 15000) combinations of scaling-factors resulted in comparable tendon-force-curves outputs. To get an idea of the results of the cost functions the combination are plotted in a color-image (For the $Bjorn_3$ data-set see figure 5.1 and for the rest see Appendix D). Every pixel in the images represent a cost-value of 1 of the predicted force curves. The color of the pixel represents the size of the cost-value (Blue = low (best), Red = high (worst)).

The estimated curve that belongs to the best cost-value of each criterium is plotted in figure 5.3. This will give a idea of the performance of the muscle model. Though for example the simple band criterium still has an 50% wrong predicted points in figure 5.2 the force curves are predicted very well for a biomechanical model.

[1]The error is the difference between measured and predicted tendon force in [N]

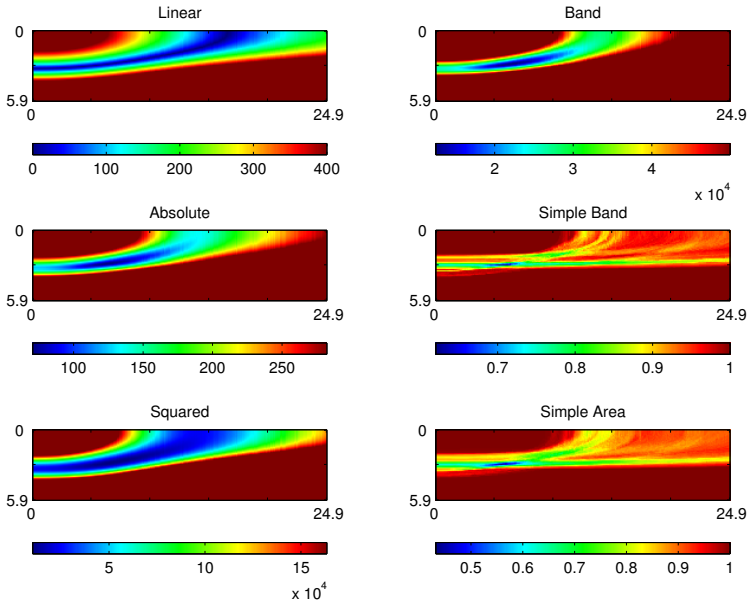

Figure 5.2: *The cost images of from the $Bjorn_3$ data-set: The pixel-axis of the images represent the scaling factor for the muscle (pixel 1 = 0, pixel 2 = 0.1, ... ,pixel 60 = 5.9, ... ,pixel 250 = 24.9).*

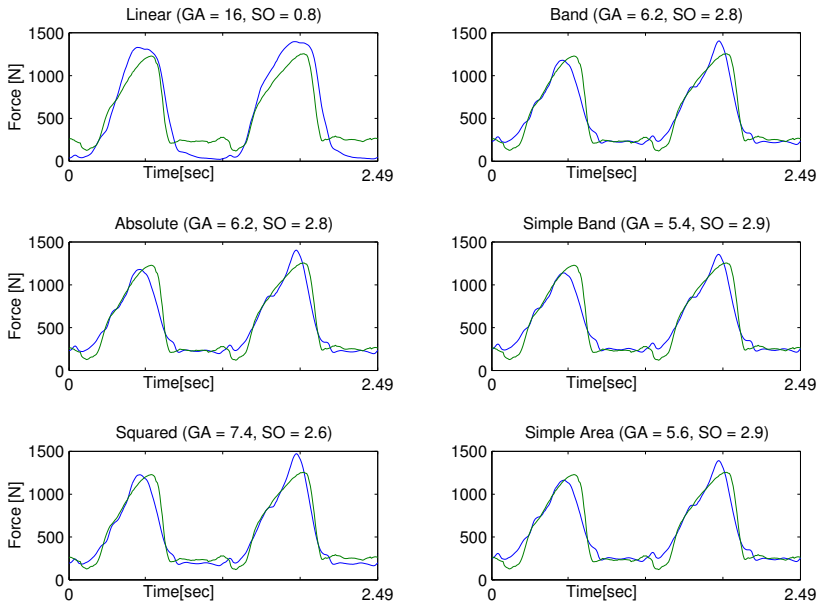

Figure 5.3: *The best predicted forces based on the minimum cost value of figure 5.2. Green = predicted, blue=measured*

As mentioned in 4.3.3 4 different tests are performed in Finland. The results of the 3 other data-sets are given in the Appendix D. These images and graphs give comparable results as in figure 5.2 and 5.3

A final verification of the muscle model that can be performed with the limited data-sets, is a

comparison between the scaling factors of the 4 different conditioned data-sets. The expectation were comparable scaling factors for all the 4 data-sets. The Absolute-criterium is used, because this gave the best plot results (see Appendix D). Other criteria are not less, but require more calculation time. It is clear that there is a difference between the 4 plots in figure 5.4 especially the scaling factors of the soleus. A reason could be the different circumstances under which the 4 data-sets were measured. But the major reason is a big difference between the EMG-offset of soleus and gastrocnemius (see figure 4.4. If there is an offset in the tendon-force this results in a much higher contribution of the soleus force. If this force-offset is less the gastrocnemius contribution increases.

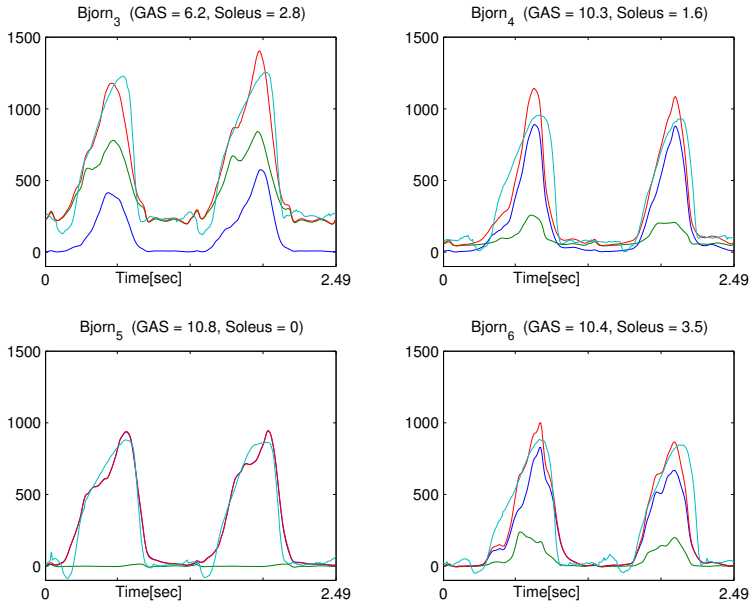

Figure 5.4: *This are best results (blue = gastrocnemius, red = estimated, green = soleus, light blue = measured*

5.2 Muscle force and movement verification

With a verified muscle model it should be possible to activated the legs with a known EMG-input. The best option was to use the EMG of Hof et al, but again the scaling/normalization of scaling factor of the EMG is unknown. The muscle length and velocity input to the muscle model is fixed to the right movement.

Many different combinations of normalization factors are tried with a simple optimalization of the these factors, but none of these combinations resulted in a good swing phase[2] and it was even not getting close to a good swing pattern. Later it appeared that the mechanical model is very sensitive, so a good tracking algorithm good find the right combination of normalization factors. But also a data-set of only 1 person could be necessary or a more specific/individual muscle with both slow and fast fibers.

[2]Because the ground contact was not working only the swing-phase is used

A second option was the use of Anybody. Because this resulted in a better output it is described in the next 2 sub-sections

5.2.1 Muscle force calculation

As mentioned in section 4.2.2 the program Anybody is able to calculate the necessary muscle-force by inverse dynamics and the min-max criterium. The same model as in SimMechanics (see figure 4.5) is implemented in Anybody. The forces are calculated with the simple muscle model of Anybody, which take only the maximum muscle force into account for the min-max criterium. A more accurate option is the advance muscle, which also takes muscle length, velocity etc. into account. Because only 6 muscle are used, this choice will not have much effect on the force estimation of the individual muscles. If there are more synergistic muscles in the model this choice has a larger effect, because not every muscle will work in his optimal operational range.

With Anybody, the first results were not the force curves as expected from the known EMG-curves. Especially the forces of the gastrocnemius and tibialis are too high. The gastrocnemius seemed to act like a knee flexor and the tibialis anterior as an actuator that prevent the foot from plantar flexion (as a reaction on the high gastrocnemius force). 5 Different setups are tested, to find the effect of the different muscles. The main reason is to see the effect on the gastrocnemius and rectus femoris, because both were too high and had a strange shape. The moment arms remain the same as mentioned in section 4.4.3

To visualize the effects of all the changes, Anybody calculated the forces during the swing phase with 5 different setups:

1. Begin situation with only the 6 muscles on the original places (resulting in a high gastrocnemius force)
2. Gastrocnemius connected to the calf, with the same distance to the ankle-joint (test the knee flexion function of this muscle
3. Setup 1 with the biceps femoris short head added to reduce the knee flexion of the gastrocnemius. This mono-articular knee flexor can visualize the effect on the Gastrocnemius force.
4. Setup 3 with the Gluteus Maximus and Illiopsoas added to help with the hip flexion and extension. These mono-articular muscles can reduce the power of the rectus femoris and hamstrings. The muscle connection points are from other Anybody models, because there was no suitable moment arm information.
5. Setup 4, but with changed the connection points around the knee of the 3 knee flexors (Gastrocnemius, Hamstrings, Biceps femoris SH) to the original Delp values. This could visualize the reduced moment arm of the gastrocnemius.

An overview of the calculated forces are visible in figures 5.5a,b and c.

From figure 5.5 a,b and c the conclusions were:

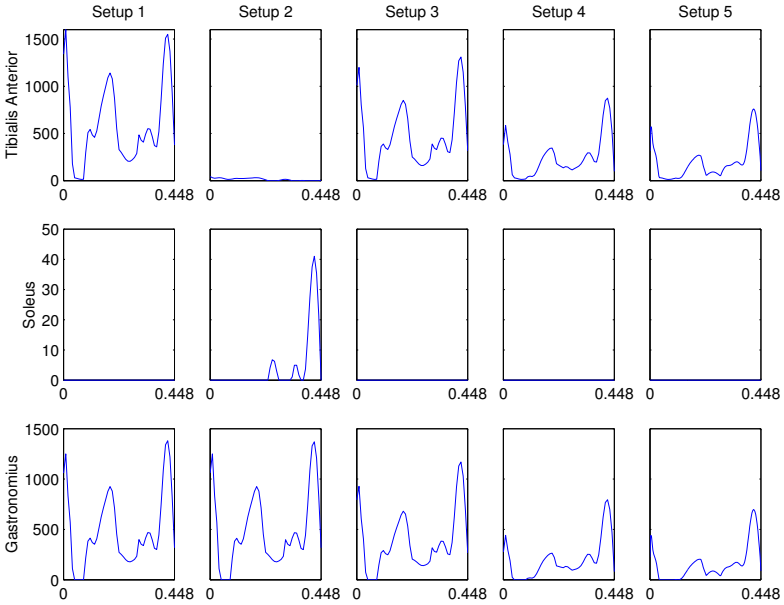

(a) For legend see below figure c on page 55

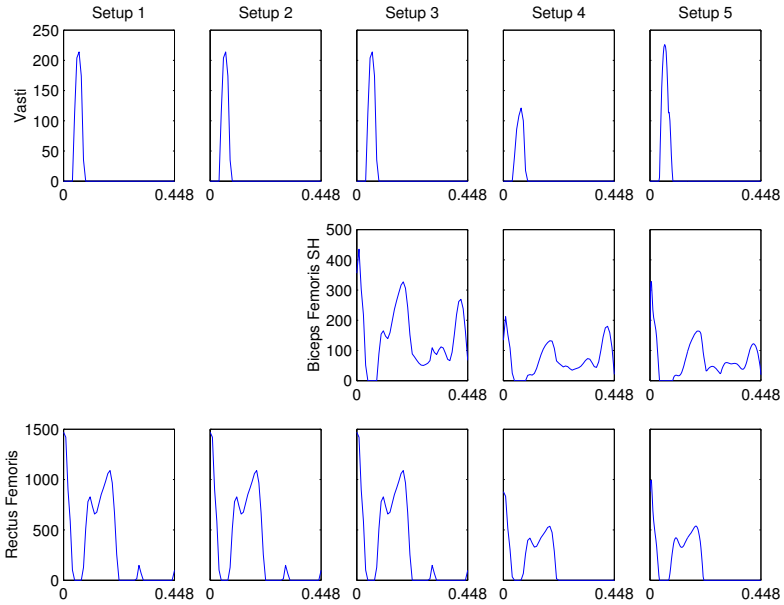

(b) For legend see below figure c on page 55

- The high Tibialis Anterior force is a reaction on the high Gastrocnemius force, because the Tibialis Anterior force is very low in Setup 2.
- The high Gastrocnemius force is only to flex the knee, because the Soleus force is not high in all the setups.
- The Biceps Femoris Short Head is not able to completely take over the Gastrocnemius force. The moment arm and/or maximum force of the Biceps Femoris are too low.
- The Hamstrings can act more like a knee flexor if the Illiopsoas is present in the model. Because the rectus femoris does not have to flex the hip alone. This also result from setup

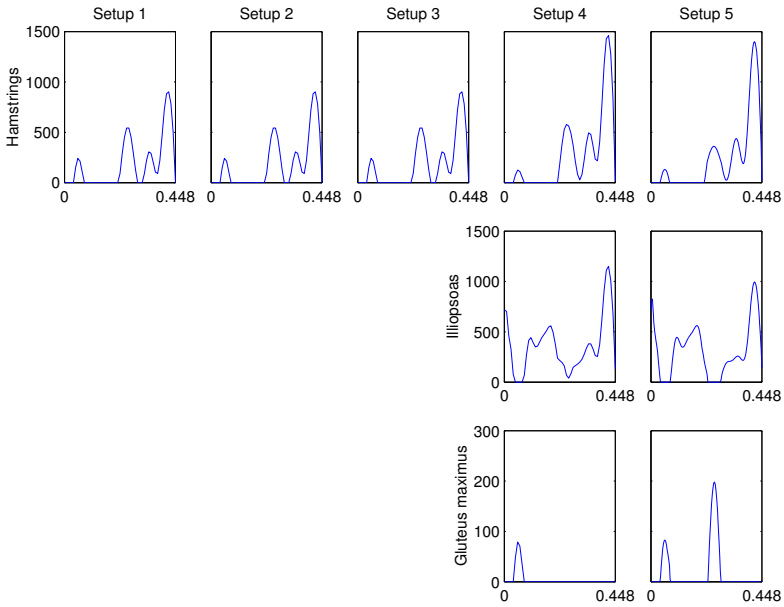

(c) For legend see below

Figure 5.5: *Force of the different leg muscles calculated by Anybody for the 5 different setups. Vertical: Muscle force [N], horizontal: Time [sec]*

3 to 4/5 in an increase of the Hamstring force and the Biceps femoris and Gastrocnemius forces decrease.

- The Rectus Femoris decreases in force with the help op the Illiopsoas. This reduces the knee extension and a reduction of the Biceps femoris and Gastrocnemius forces.
- The influence of the Gluteus maximus is not so high in the swing phase, or the moment arm is too high. This could not be verified.

In figure 5.6 there is an overview of the 9 lower leg muscles with the data-set used in setup 5. Though the shapes are still not completely comparable it is already much better than with setup 1. The major reason for the difference is the co-contraction of some muscle, which not always results in a movement but only in a stiffer joint. Anybody does not take this effect into account. Therefore could these force curves be a starting point to find the real force with extra EMG information.

5.2.2 Validation with SimMechanics

After the tests in Anybody, the results have to be tested in SimMechanics. Because the models are completely the same it should result in the right movements. First, setup 2 is used to test the link between Anybody and SimMechanics is working, because mono-articular muscles do not pass on a small error directly. Second, setup 5 is used to see the effect with all the 9 muscles.

During the verification of setup 2 a strange effect is noticed. The force input from Anybody had 51 samples in the swing phase and after 50% of the simulation time the joint-angles drifted

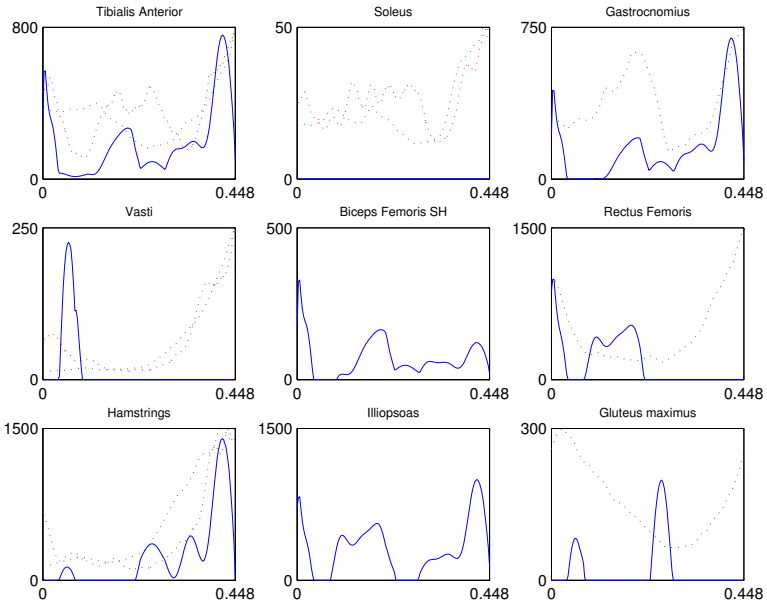

Figure 5.6: *Overview of the 9 muscle forces (=blue) of Setup 5. For some muscles I add the EMG shape measured by Hof (=green) of by Spauch(=red)*

away from the intentional value. By increasing the number of samples to 251 the drift was almost gone and good enough for this simulation (see figure 5.7).

With the result of figure 5.7 the number of samples for setup are set to 251. The beginning of setup 5 is very promising, but after 0.15 sec the ankle acceleration makes a mistake and this has its influence on the rest of the simulation. A change to 449 samples had no better effect on the movement. An earlier test of 151 samples gave even a better result, but drifted also on the same point only in the other direction (see figure 5.8). The expectation of an optimal number of samples between the 151 and 251 samples resulted in nothing. Even 152 samples gave an error in the same direction as the 251. And sometimes complete different movement curve was the result with specific number of samples.

Apparently is the mechanical model in SimMechanics very sensitive in the forward path. Though the force curves of Anybody do not change in shape, they have only a small detailed change, because of the higher resolution (by increase of the number of samples). Maybe the error is has a numerical origin in Simulink, or the force is not calculated accurate enough. Shortage of time prevented a good solution for this problem.

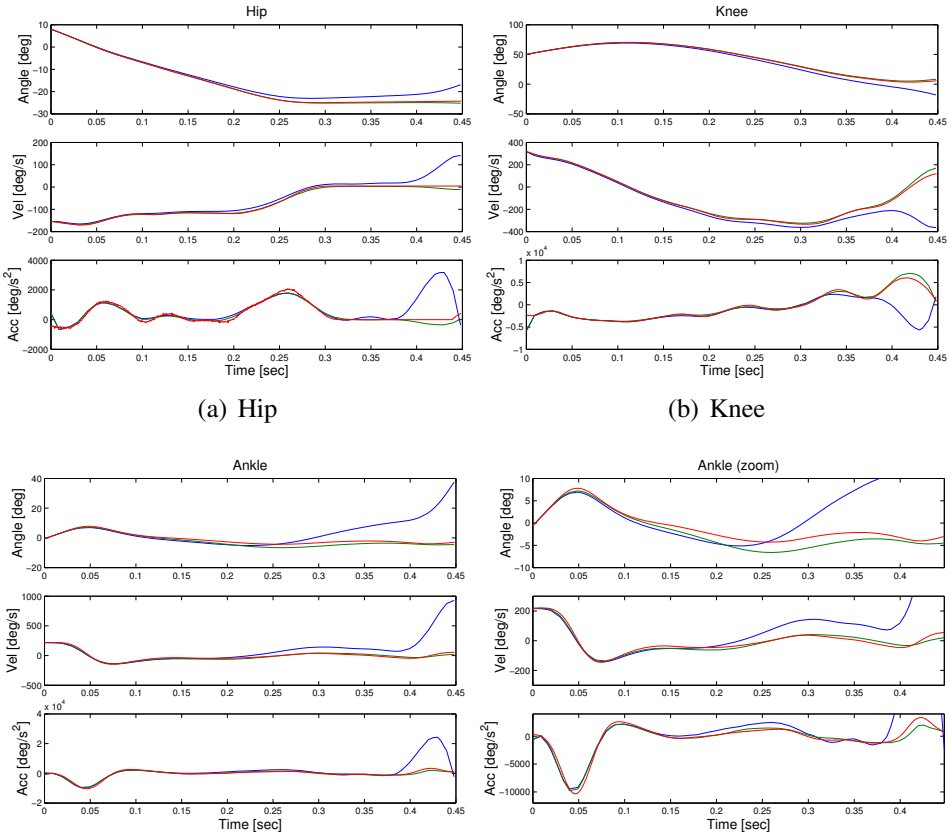

(a) Hip (b) Knee

(c) Ankle (d) Ankle(zoom)

Figure 5.7: *Results of setup 2 calculated force in used in SimMechanics. Blue = force activated (51 samples), Green=(251 samples), Red= intentional swing*

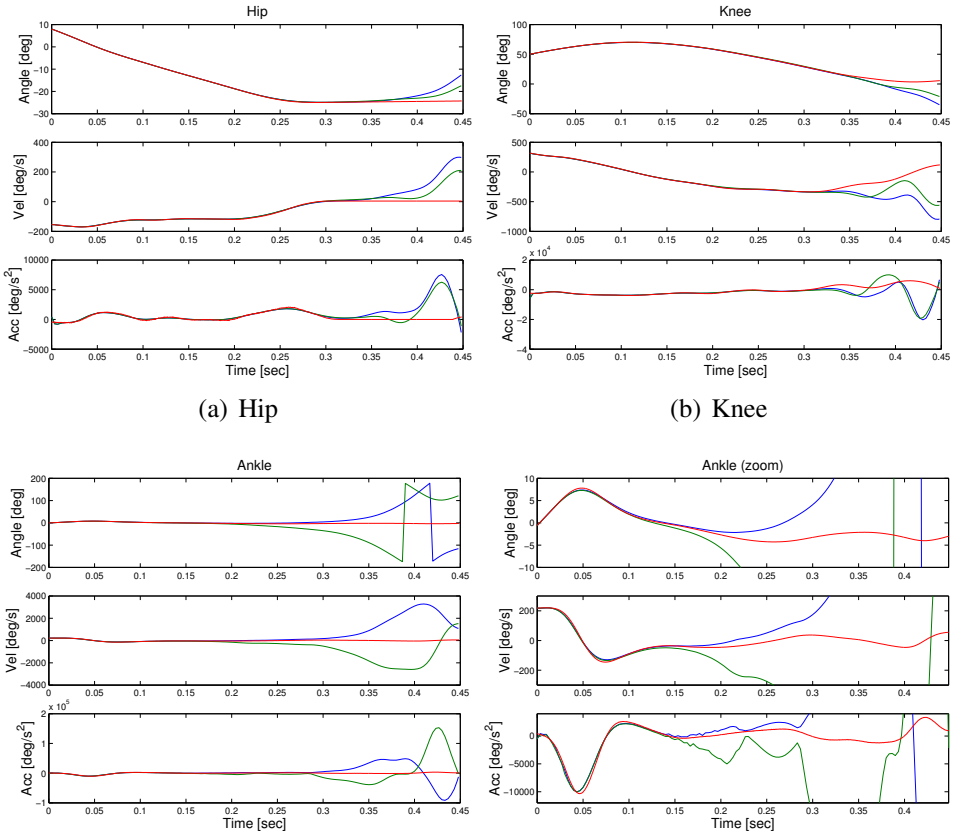

(a) Hip (b) Knee

(c) Ankle (d) Ankle(zoom)

Figure 5.8: emphResults of setup 5 calculated force in used in SimMechanics. Blue = force activated (151 samples), Green=(251 samples), Red= intentional swing

CHAPTER 6

Conclusion

The original intention of this project was to answer the questions: "What happens when part of the feedback is turn on and off? and what happens if the feedback in partly turned on?". Due to several problems with the software, previous work and available data these questions could not be answered. Nevertheless a few conclusions can be made based on the verifications and experience gained in this project.

During the project the use of SimMechanics for the mechanical modelling was not always easy, but in the end is a a very useful program to model a mechanical model. It is easy to use (especially when you are not a mechanical engineer), compared to modelling with Lagrance equations for example. The only missed option is a collision detection optimalization for the ground contact, but maybe this will be available in future releases. Also a very fast computer can be very helpful during the simulations. Together with Matlab it is a good/cheap package to develop a simulation-program, which can be used by several researchers. Finally, the designer only has to be very careful with designing the model, because it is not always obvious what is happening inside the block.

The muscle model can predict a muscle force. Although it is not exactly sure if this is the right relation, because a combination of 2 EMG-inputs and one force-output is used. Also too much parameters are adjusted to say the model is perfect. Maybe is a more muscle specific muscle with fast and slow fibers and many motor unit is better. With the article of Cheng et al. [12] this can not be a problem.

The forward dynamics activation is more difficult than first thought and especially very sensitive to small difference. The general opinion that many forces results in the same movement, but with this model and verification this is maybe not so very true. The major reason for this instability is a absence of any feedback when small errors occur, which have large effects on the moment arm. The next step in expanding the model can solve this problem with the imple-

mentation of the neural feedback.

To find a the muscle forces Anybody could be very useful. Though the force do not match to the EMG-input, they give a good starting-point for the muscle force. Anybody also showed that is more realistic to implement a 9 muscle lower leg model with a biarticular and monoarticular muscle for every joint.

CHAPTER 7

Recommendation

With the experience gained in this project for setting up a complete computer model for simulating the human locomotion, I would suggest the following continuation of the project.

To be able to validate a model input-output verification data is necessary. Before this project the idea was this data is widely available. This is partly true, but not a complete data set is found with all the necessary signals/quantities. The data-set needs the following data based on one person or group of persons measured all under the same conditions.

- Anthropometry
- EMG
- Joint angles or positions
- Tendon force (to validate neural part)
- Ground reaction force

More data-sets with other conditions can be useful, but with the complexity of the complete model a validation based on 1 condition is already a huge amount of data. A data-set based on a group of persons is more important, because the model is first needed to answer a general answer and not based on one person.

The mechanical model appear to be very sensitive in the forward activation. As mentioned in the conclusion for the the reason is the small error in the moment arm which can have a large effect on the joint acceleration, which will increase the moment error. Normally a feedback loop is able to stabilize a system. A human has many sensors to correct for the small errors. In this model the complete neural feedback could be used for the stabilization. The first start can be the mathematical transfer functions mentioned in this report.

For a complete walking model also a good ground-model is necessary. During this project the

feedback of the model was too high frequent, which slows down the simulation speed dramatically. A low pass filter in the reaction force could be a solution, or maybe a complete other approach for this problem.

Bibliography

[1] http://isb.ri.ccf.org/data/.

[2] http://www.anybodytech.com.

[3] http://www.mathworks.com/products/simmechanics/.

[4] Frank C. Anderson and Marcus G. Pandy. Dynamic optimization of human walking. *?*, ?

[5] R.A. Brand, D.R. Pedersen, and J.A. Friederich. The sensitivity of muscle force predictions to changes in physiologic cross-sectional area. *Journal of Biomechanics*, 19:589–596, 1986.

[6] Ian E. Brown and Gerald E. Loeb. Measured and modeled properties of mammalian skeletal muscle. II the effects of stimulus frequency on force-length and force-velocity relationships. *Journal of Muscle Research and Cell Motility*, 20:627–643, 1999.

[7] Ian E. Brown and Gerald E. Loeb. Measured and modeled properties of mammalian skeletal muscle. I the effects of post-activation potentiation on the time course and velocity dependencies of force production. *Journal of Muscle Research and Cell Motility*, 20:443–456, 1999.

[8] Ian E. Brown and Gerald E. Loeb. Measured and modeled properties of mammalian skeletal muscle: IV dynamics of activation and deactivation. *Journal of Muscle Research and Cell Motility*, 21:33–47, 2000.

[9] Ian E. Brown and Gerald E. Loeb. Measured and modeled properties of mammalian skeletal muscle: III the effects of stimulus frequency on stretch-induced force enhancement and shortening-induced force depression. *Journal of Muscle Research and Cell Motility*, 21:21–31, 2000.

[10] William L. Buford, F. Marty Ivey, J. Dan Malone, Rita M. Patterson, Gregory L. Peare, Doan K. Nguyen, and Anthony A. Stewart. Muscle balance at the knee moment arms for

the normal knee and the acl-minus knee. *IEEE TRANSACTIONS ON REHABILITATION ENGINEERING*, 5(4):367–379, 1997.

[11] W.J. Chen and R.E. Poppele. Small-signal analysis of response of mammalian muscle spindles with fusimotor stimulation and a comparison with large-signal responses. *Journal of Neurophysiology*, 41(1):15–27, 1978.

[12] Ernest J. Cheng, Ian E. Brown, and Gerald E. Loeb. Virtual muscle: a computational approach to understanding the effects of muscle properties on motor control. *Journal of Neuroscience Methods*, 101:117–130, 2000.

[13] Patrick E. Crago. *Creating Neuromusculoskeletal Models*, pages 119–133. In [58], 2000.

[14] A.G. Cresswell, W.N. Löscher, and A. Thorstensson. Influence of gastrocnemius muscle length on triceps surae torque development and electromyographic activity in man. *Experimental Brain Research*, 105:283–290, 1995.

[15] Christopher L Vaughant'and Brian L Davis and Jeremy C O'Connor. *Dynamics of Human Gait*. Kiboho Publishers, Cape Town, South Africa, 2nd edition edition, 1999.

[16] Scott L. Delp, J. Peter Loan, Melissa G. Hoy, Felix E. Zajac, Eric L. Topp, and Joseph M. Rosen. An interactive, graphics-based model of the lower extremity to study orthopaedic surgical procedures. *IEEE Transactions on Biomedical Engineering*, 37(8):557–567, August 1990.

[17] M. Epstein and W. Herzog. *Theoretical Models of Skeletal Muscle*. John Wiley & sons, 1998.

[18] Z. Hasan. A model of spindle afferent response to muscle stretch. *Journal of Neurophysiology*, 49(4):989–1003, April 1983.

[19] W. Herzog and L.J. Read. Lines of action and moment arms of the major force-carrying structures crossing the human knee joint. *Journal of Anatomy*, 182:213–230, 1993.

[20] W. Herzog, L.J. Read, and H.E. ter Keurs. Experimental determination of force-length relations of intact human gastrocnemius muscles. *Clinical Biomechanics*, 6:230–238, 1991.

[21] A.V. Hill. Then heat of shortening and the dynamic constants of a muscle. *Proceedings of the Royal Society*, 126B:136–195, 1938.

[22] A.L. Hof, H. Elzinga, W. Grimmius, and J.P.K. Halbertsma. Speed dependence of averaged emg profiles in walking. *Gait & Posture*, 16(1):78–86, aug 2002.

[23] J.C. Houk, W.C. Rymer, and P.E. Crago. Dependece of dynamic response of spindle receptors on muscle length and velocity. *Journal of Neurophysiology*, 46(1):143–166, July 1981.

[24] J.C. Houk and W. Simon. Responses of golgi tendon organs to froces applied to muscle tendon. *Journal of Neurophysiology*, 30:1466–1481, 1967.

[25] M.G. Hoy, F.E. Zajac, and M.E. Gordon. A musculoskeletal model of the human lower extremity: the effect of muscle, tendon, and moment arm on the moment-angle relationship of musculotendon actuators at the hip, knee, and ankle. *Journal of Biomechanics*, 23:157–169, 1990.

[26] Jean-Baptiste Huber. Descriptive versus soft models of muscle under FES. Master's thesis, Department of Health Science and Technology, Aalborg University, 2002.

[27] Peter A. Huijing. *Modeling of Homogeneous Muscle: Is It Realistic ot Consider Skeletal Muscle as a Lumped Sarcomere of Fiber*, pages 92–98. In [58], 2000.

[28] A.F. Huxley. Muscle structure and theories of contraction. *Progress in Biophysics and Chemistry*, 7:257–318, 1957.

[29] Y. Ichinose, Y. Kawakami, M. Ito, and T. Fukunaga. Estimation of active force-length characteristics of human vastus lateralis muscle. *Acta Anat.(Basel.)*, 159:78–83, 1997.

[30] V.T. Inman, H.J. Ralston, and F. Todd. *Human walking*. Williams & Wilkins, Baltimore, 1981.

[31] Eric R. Kandel and James H. Schwartz adn Thomas M. Jessell. *Priciples of Neural Science*. McGraw-Hill Companies, Inc., 1999.

[32] Chris Kirtley and Michael W Whittle. Influence of walking speed on gait parameters. *Journal of Biomedical Engineering*, 7:282–288, 1985.

[33] Constantinos N. Maganaris. In vivo measurement-based estimations of the moment arm in the human tibialis anterior muscle-tendon unit. *Journal of Biomechanics*, 33:375–379, 2000.

[34] Constantinos N. Maganaris. Force-length characteristics of in vivo human skeletal muscle. *Actual Physiology Scandinavia*, 172:279–285, 2001.

[35] Constantinos N. Maganaris, Vasilios Baltzopoulos, and Anthony J. Sargeant. In vivo measurement-based estimations of the human achilles tendon moment arm. *Eur Journal of Applied Physiology*, 83:363–369, 2000.

[36] E. Marsh, D. Sale, A.J. McComas, and J. Quinlan. Influence of joint position on ankle dorsiflexion in humans. *Journal of Applied Physiology*, 51:160–167, 1981.

[37] P.B.C. Matthews and R.B. Stein. The sensitivity of muscle spindle afferents to small sinusoidal changes of length. *Journal of Physiology*, 200:723–743, 1969.

[38] Naomichi Ogihara and Nobutoshi Yamazaki. Generation of human bipedal locomotion by a bio-mimetic neuro-musculo-skeletal model. *Biological Cybernetics*, 84:1–11, 2001.

[39] C. Pop, A. Khajepour, J.P. Huissoon, and A.E. Patla. Application of bondgraphs to human locomotion modelling. *?*, ?

[40] Dejan Popović and Thomas Sinkjær. *Control of Movement for the Physically Disabled*. Springer-Verlag, London, 2000.

[41] R.E. Popple and R.J. Bouwman. Quantitative description of linear behavior of mammalian muscle spindles. *Journal of Neurophysiology*, 33:59–72, 1970.

[42] Arthur Prochazka. Proprioceptive feedback and movement regulation. In L. Rowell and T. Sheperd, editors, *Handbook of Physiology. Section 12. Exercise: Regulation and Integration of Multiple Systems*, chapter 3, pages 89–127. American Physiological Society, New York, 1996.

[43] Arthur Prochazka. Quantifying proprioception. In M.D. Binder, editor, *Progress in Brain Research*, volume 123, chapter 11, pages 133–142. Elsevier Science BV, 1999.

[44] Arthur Prochazka, Deborah Gillard, and David J. Bennett. Implications of positive feedback in the control of movement. *Journal of Neurophysiology*, 77:3237Ű3251, 1997.

[45] Arthur Prochazka, Deborah Gillard, and David J. Bennett. Positive force feedback control of muscles. *Journal of Neurophysiology*, 77:3226Ű3236, 1997.

[46] Arthur Prochazka and Monica Gorassini. Ensemble firing of muscle afferents recorded during normal locomotion in cats. *Journal of Physiology*, 507.1:293–304, 1998.

[47] Arthur Prochazka and Monica Gorassini. Models of ensemble firing of muscle spindle afferents recorded during normal locomotion in cats. *Journal of Physiology*, 507.1:277–291, 1998.

[48] Arthur Prochazka and Sergiy Yakovenko. Locomotor control: From spring-like reactions of muscles to neural prediction. In Nelson J. Randall, editor, *The Somatosensory System*. CRC Press, Boca Raton (Florida), 2002.

[49] D. Sale, J. Quinlan, E. Marsh, A.J. McComas, and A.Y. Belanger. Influence of joint position on ankle plantarflexion in humans. *Journal of Applied Physiology*, 52:1636–1642, 1982.

[50] S.S. Schäfer. The discharge frequencies of primary muscle spindle endings during simultaneous stimulation of two fusimotor fibres. *Plügers Archiv*, 350:359–372, 1974.

[51] Lauralee Sherwood. *Human Physiology - From Cells to Systems*. Brooks/Cole, Pacific Grove, CA, USA, 4th edition, 2001.

[52] Filipe M. Silva and J.A. Tenreiro Machado. Hybrid position/force algorithms for biped locomotion. *?*, ?

[53] S.A. Spector, P.F. Gardiner, R.F. Zernicke, R.R. Roy, and V.R. Edgerton. Muscle architecture and force-velocity characteristics of cat soleus and medial gastrocnemius: implications of neural control. *Journal of Neurophysiology*, 44:951–960, 1980.

[54] Frans C.T. van der Helm and Leonard A. Rozendaal. *Musculoskeletal Systems with Intrinsic and Proprioceptive Feedback*, pages 164–174. In [58], 2000.

[55] Thomas L. Wickiewicz, Roland R. Roy, Perry L. Powell, and V. Reggie Edgerton. Muscle architecture of the human lower limb. *Clinical Orthopaedics and Related Research*, 179:275–283, 1983.

[56] David A. Winter. *Biomechanics and Control of Human Movement*. John Wiley & Sons, Inc., New York, 2nd edition, 1990.

[57] Jack M. Winters. *Subtle Nonlinear Neuromuscular Properties Are Consistent with Teleological Design Principles*, pages 100–116. In [58], 2000.

[58] Jack M. Winters and Patrick E. Crago. *Biomechanics and Neural Control of Posture and Movement*. Springer-Verlag, New York, 2000.

[59] Jack M. Winters and Lawrence Stark. Analysis of fundamental human movement patterns through the use of in-depth antagonistic muscle models. *IEEE Transactions on Biomedical Engineering*, BME-32(10):826–839, 1985.

[60] G.I. Zahalak and S.-P. Ma. Muscle activation and contraction: constitutive relations based directly on cross-bridge kinetics. *Journal of Biomechanical Engineering*, 112:52–62, 1990.

[61] F.E. Zajac. Muscle and tendon: Properties, models, scaling, and application to biomechanics and motor control. *Critical Reviews in Biomedical Engineering*, 17(4):359–411, 1989.

APPENDIX A

Appendix EMG

All the used and verified EMG in the project

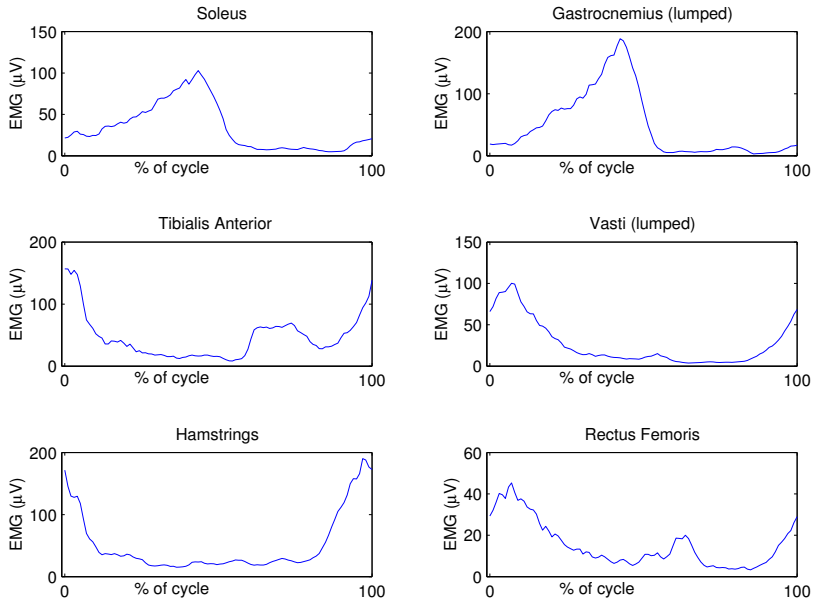

Figure A.1: *The EMG-curves form the 6 muscles that are used in the beginning of the project. From Hof et al. [22]*

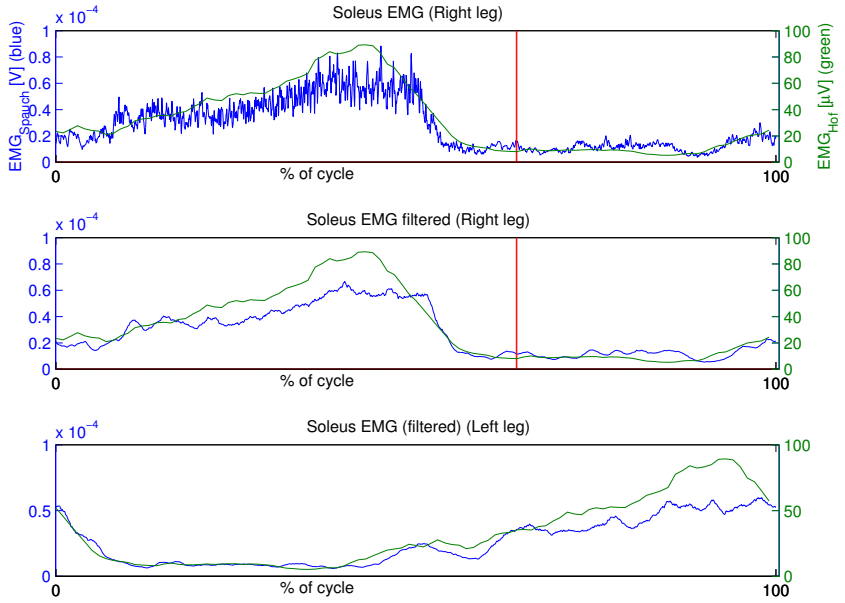

Figure A.2: *Comparison between the Soleus EMG of Hof et al. and Spauch*

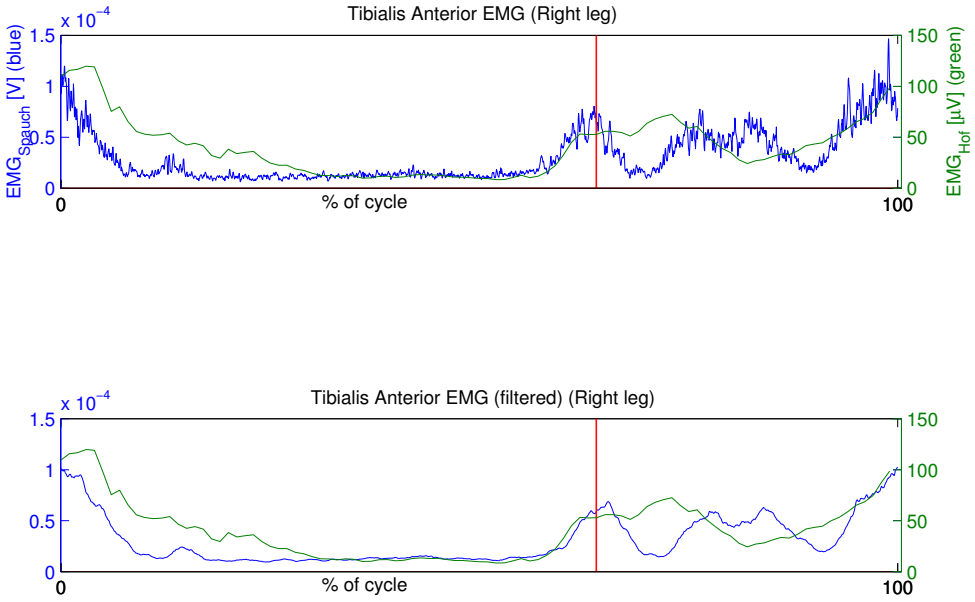

Figure A.3: *Comparison between the Tibialis Anterior EMG of Hof et al. and Spauch*

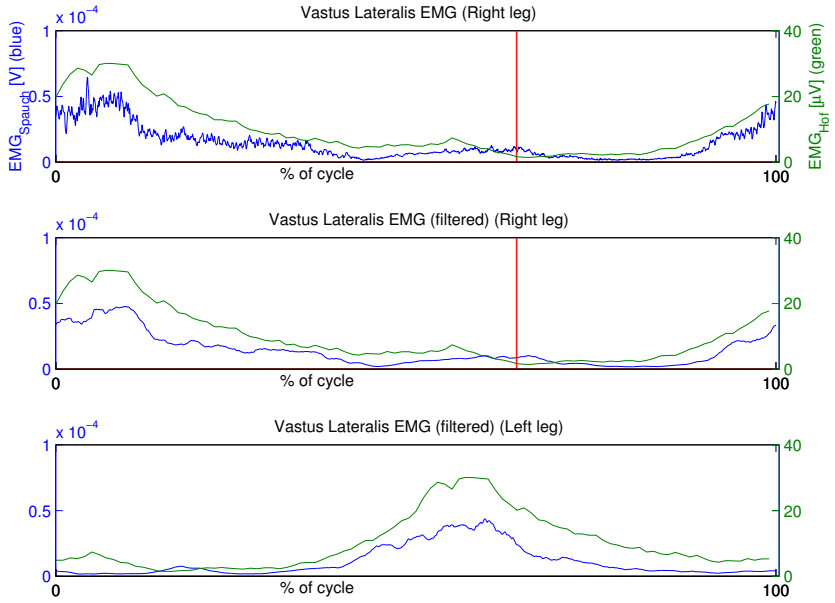

Figure A.4: *Comparison between the Vastus Lateralis EMG of Hof et al. and Spauch*

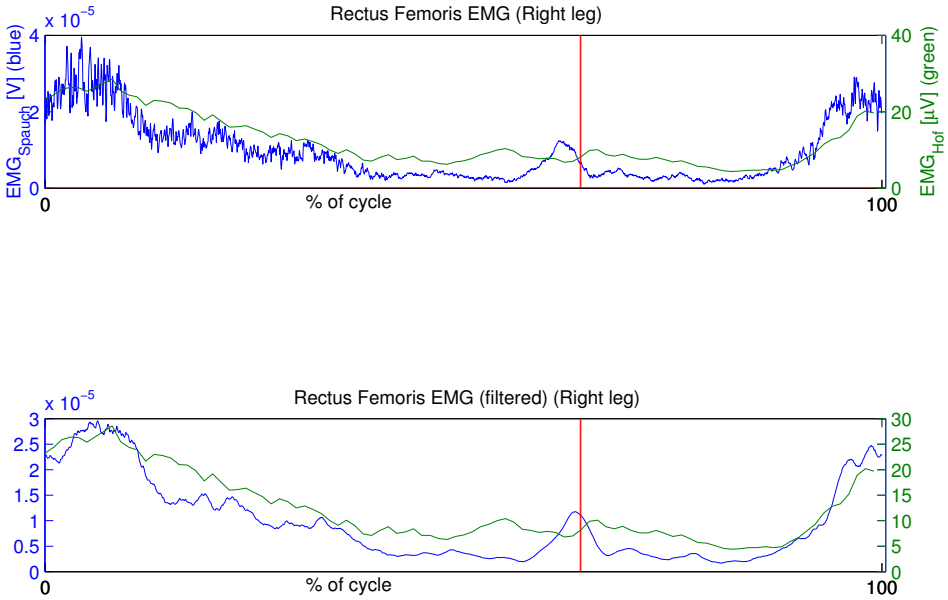

Figure A.5: *Comparison between the Rectus Femoris EMG of Hof et al. and Spauch*

APPENDIX B

Muscle model

The parameters form the articles of Brown and Loeb ([7], [6], [9] and [8]) , Cheng et al. [12] and used in this project averaged with the values from Cheng et al. (10% super slow, 40% slow fibers and 50% fast fibers) as listed in table. After the table the different curves of the muscle model are given. To see a difference between Cheng et al. his slow and fast fibers are also plotted.

Variable	Dimension	**Cat**		**Human**			**This Project**
		Slow	Fast	Super Slow	Slow	Fast	
a_f	[-]	0.56	0.56	0.56	0.56	0.56	0.56
a_{s1}	[-]	1	1	1	1	1.76	-
a_{s2}	[-]	1	1	1	1	0.96	-
a_{v0}	[-]	-4.7	-1.53	-4.7	-4.7	-1.53	-4.7
a_{v1}	[-]	8.41	0	8.41	8.41	0	8.41
a_{v2}	[-]	-5.34	0	-5.31	-5.31	0	-5.31
b_v	[-]	0.18	1.05	0.1747	0.3494	0.6864	0.52
c_1	[-]	42.3[1]	166.2[2]	23	23	23	23
c_2	[-]	-0.020	-0.020	-0.020	-0.020	-0.020	-
c^T	[-]	27.8	27.8	27.8	27.8	27.8	27.8
c_{v0}	[-]	5.88	-3.21	5.88	5.88	-5.7	0.1
c_{v1}	[-]	0	4.17	0	0	9.18	4.6
c_Y	[-]	0.35	0	0.35	0.35	0	-
k_1	[-]	0.054[3]	0.050[4]	0.046	0.046	0.046	0.046
k_2	[-]	-18.7	-18.7	-21.0375	-21.0375	-21.0375	-
k^T	[-]	0.0047	0.0047	0.0047	0.0047	0.0047	0.0047
L_{r1}	$[L_o]$	1.46[5]	1.39[6]	1.17	1.17	1.17	1.17
L_{r2}	$[L_o]$	0.79	0.79	0.7022	0.7022	0.7022	-
L_r^T	$[L_o]$	0.964	0.964	0.964	0.964	0.964	0.964
n_{f0}	[-]	2.11	2.11	2.11	2.11	2.11	2.11
n_{f1}	[-]	5	3.31	5	5	3.31	4.15
T_{f1}	[msec]	48.4	12.1	68.5667	34.2833	20.5700	30.88
T_{f2}	[msec]	32.0	8.0	45.3333	22.6667	13.6000	21.14
T_{f3}	[msec]	66.4	16.6	94.0667	47.0333	28.2200	42.20
T_{f4}	[msec]	35.6	8.9	50.4333	25.2167	15.1300	22.63
T_L	[msec]	0.0880	0.0880	0.0880	0.0880	0.0880	0.0880
T_S	[msec]	-	43	-	-	43	-
T_Y	[msec]	200	-	200	200	-	-
V_{max}	$[L_o/s]$	-4.70	-7.39	-3.9400	-7.8800	-9.1516	-8.5
V_Y	$[L_o/s]$	0.1	-	0.1	-	-	-
β	[-]	2.3	1.55	2.3	2.3	1.55	1.93
η	[Ns/m]	-	-	0.01	0.01	0.01	0.01
ρ	[-]	1.62	2.12	1.62	1.62	2.12	1.87
ω	[-]	1.26	0.81	1.1244	1.1244	0.7463	0.93

Table B.1: The muscle parameters of the cat (from [7], [6], [9] and [8]), human fibers [12] and this project

[1] average of 25.6, 31.8, 69.6
[2] average of 67.1, 76.4, 355
[3] average of 0.046, 0.058, 0.059
[4] average of 0.040, 0.053, 0.056
[5] average of 1.34, 1.50, 1.54
[6] average of 1.35, 1.40, 1.41

B.1 Muscle model curves

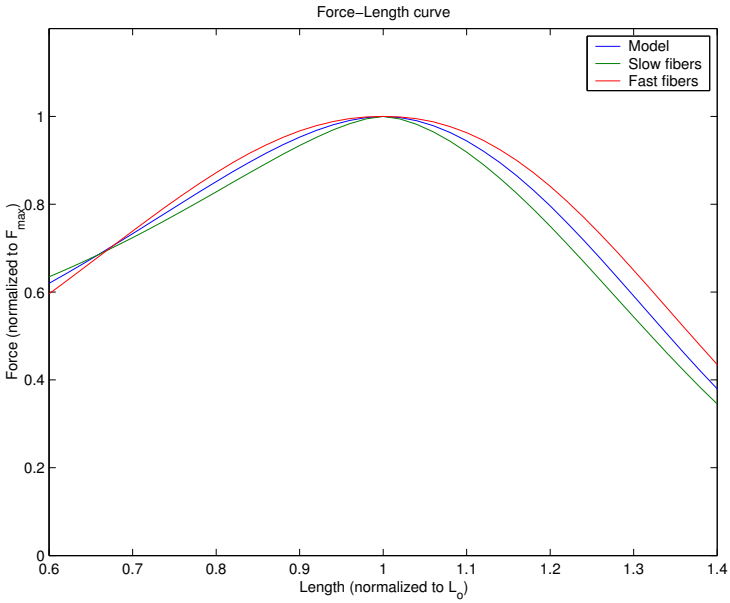

Figure B.1: *Force-length relation of the contractile element*

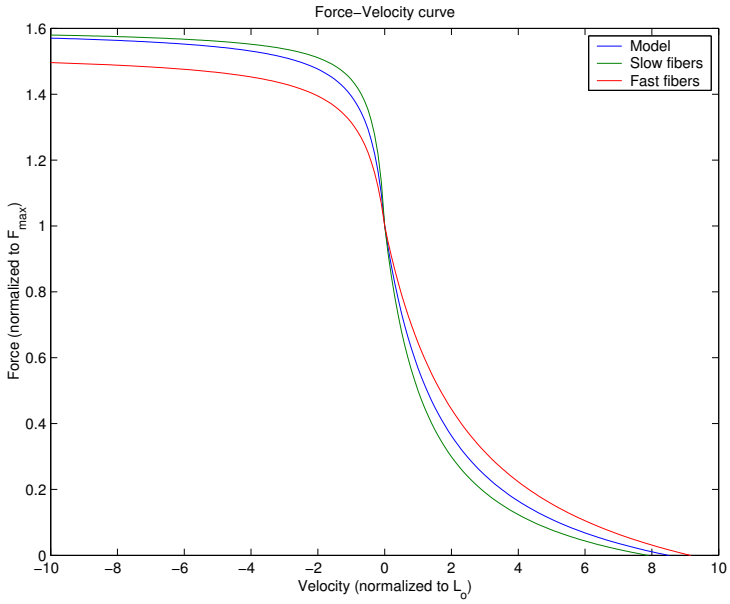

Figure B.2: *Force-velocity relation of the contractile element*

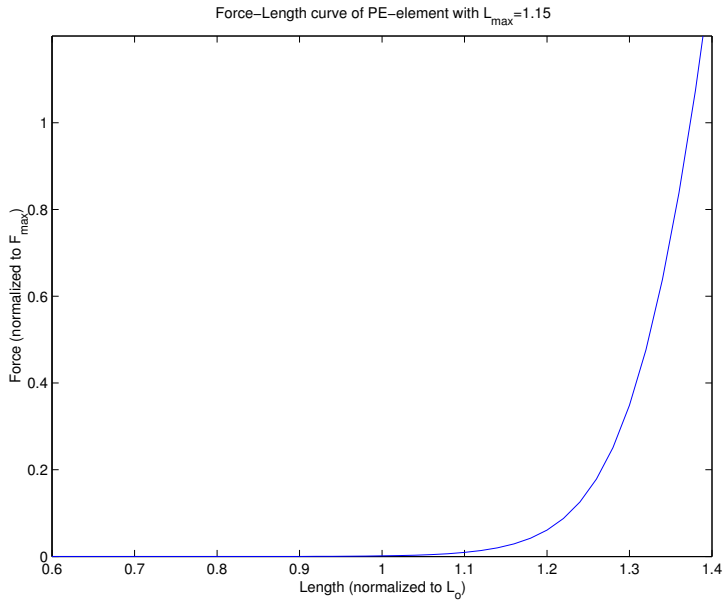

Figure B.3: *Force-length relation of the passive element*

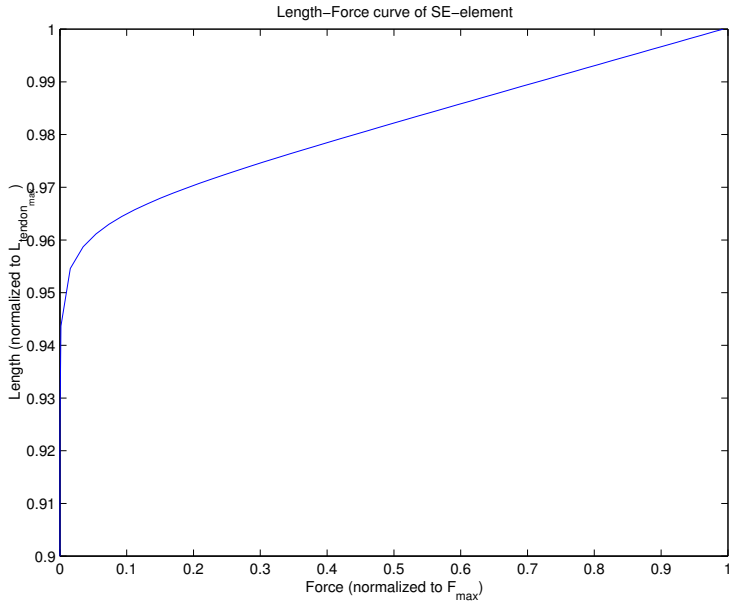

Figure B.4: *Length-force relation of the serial element*

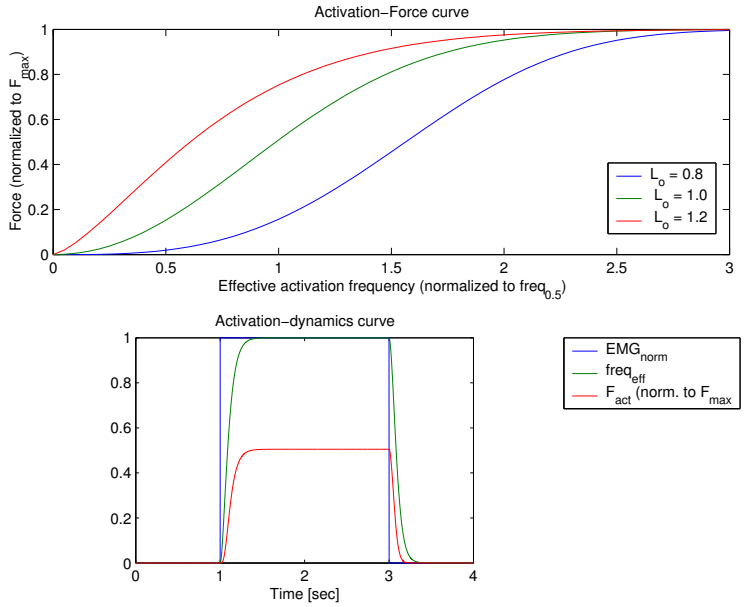

Figure B.5: *The non-linear activation dynamics to see the Force-frequency-length relation and the step response of the activation block (Unit-step of the EMG, $L = L_o$, V = 0)*

APPENDIX C

Muscle anthropometry

All the muscle parameters needed for the implementation. From F_{max} to all the verified muscle connection points

	F_{max} [N]	Pennation angle [deg]	L_o [m]
Soleus	**2839**	**25.0**	**0.0300**
Gastrocnemius MH	1113	17.0	0.0450
Gastrocnemius LH	488	8.0	0.0640
Gastrocnomi	**1601**	**14.3**	**0.0508**
Tibialis Anterior	**603**	**5.0**	**0.0980**
Vastus Medialis	1294	5.0	0.0890
Vastus Lateralis	1871	5.0	0.0840
Vastus Intermedius	1365	3.0	0.0870
Vasti	**4530**	**4.4**	**0.0863**
Biceps Femoris SH	**402**	**23.0**	**0.1730**
Biceps Femoris LH	717	0.0	0.1090
Semitendinosus	328	5.0	0.2010
Semimembranosus	1030	15.0	0.0800
Hamstrings	**2059**	**8.2**	**0.1091**
Rectus Femoris	**779**	**5.0**	**0.0840**
Gluteus Maximus(1)	382	5.0	0.1420
Gluteus Maximus(2)	546	0.0	0.1470
Gluteus Maximus(3)	368	5.0	0.1440
Gluteus Maximus	**1296**	**2.9**	**0.1447**
Iliacus	429	7.0	0.1000
Psoas	371	8.0	0.1040
Illiopsoas	**800**	**7.5**	**0.1019**

Table C.1: Muscle parameters from muscles used in this project

	Origin	X [m]	Y [m]	Z [m]	Insertion	X [m]	Y [m]	Z [m]
Soleus	Tibia	-0.0024	-0.1533	0.0071	Calcn	0.0044	0.0310	-0.0053
Gastrocnemius MH	Femur	-0.0127	-0.3929	-0.0235	Calcn	0.0044	0.0310	-0.0053
Gastrocnemius LH	Femur	-0.0155	-0.3946	0.0272	Calcn	0.0044	0.0310	-0.0053
Gastrocnemi	Femur	-0.0136	-0.3934	-0.0077	Calcn	0.0044	0.0310	-0.0053
Tibialis Anterior	Tibia	0.0179	-0.1624	0.0115	Calcn	0.1166	0.0178	-0.0305
Biceps Femoris SH	Femur	0.005	-0.2111	0.0234	Tibia	-0.0101	-0.0725	0.0406
Vastus Medialis	Femur	0.0140	-0.2099	0.0188	Patella	0.0063	0.0445	-0.0170
Vastus Lateralis	Femur	0.0048	-0.1854	0.0349	Patella	0.0103	0.0423	0.0141
Vastus Intermedius	Femur	0.0290	-0.1924	0.0310	Patella	0.0058	0.0480	-0.0006
Vasti	Femur	0.0147	-0.1945	0.0291	Patella	0.0078	0.0446	0.0008
Biceps Femoris LH	Pelvis	-0.1244	-0.1001	0.0666	Tibia	-0.0081	-0.0729	0.0423
Semitendinosus	Pelvis	-0.1237	-0.1043	0.0603	Tibia	0.0027	-0.0956	-0.0193
Semimembranosus	Pelvis	-0.1192	-0.1015	0.0695	Tibia	-0.0024	-0.0536	-0.0194
Hamstrings	Pelvis	-0.1217	-0.1015	0.0670	Tibia	-0.0036	-0.0669	0.0019
Rectus Femoris	Pelvis	-0.0295	-0.0311	0.0968	Patella	0.0121	0.0437	-0.0010

Table C.2: The muscle connection points. Data obtained from Delp with little adjustments to correct for the moment arms

	Origin	X [m]	Y [m]	Z [m]	Insertion	X [m]	Y [m]	Z [m]
Soleus	Knee	-0.0024	-0.1533	0.0071	Ankle	-0.0444	-0.0110	0.0027
Gastrocnemi	Hip	-0.0136	-0.4513	-0.0080	Ankle	-0.0444	-0.0110	0.0027
Tibialis Anterior	Knee	0.0179	-0.1624	0.0115	Ankle	0.0678	-0.0242	-0.0226
Biceps Femoris SH	Hip	0.0050	-0.2422	0.0234	Knee	-0.0101	-0.0725	0.0406
Vasti	Hip	0.0147	-0.2231	0.0291	Knee	0.0522	0.0231	-0.0016
Hamstrings	Hip	-0.0510	-0.0354	-0.0165	Knee	-0.0036	-0.0669	0.0019
Rectus Femoris	Hip	0.0412	0.0350	0.0133	Knee	0.0565	0.0222	-0.0034

Table C.3: Adjusted connection points from Delp

	Origin	X [m]	Y [m]	Z [m]	Insertion	X [m]	Y [m]	Z [m]
Soleus	Knee	-0.0024	-0.1533	0	Ankle	-0.0529	-0.0170	0
Gastrocnemi	Hip	-0.0126	-0.4287	0	Ankle	-0.0529	-0.0170	0
Tibialis Anterior	Knee	0.0179	-0.1624	0	Ankle	0.0438	-0.0122	0
Biceps Femoris SH	Hip	-0.0370	-0.2422	0	Knee	-0.0091	-0.0235	0
Vasti	Hip	0.0147	-0.2231	0	Knee	0.0342	0.0206	0
Hamstrings	Hip	-0.0561	-0.0579	0	Knee	-0.0066	-0.0321	0
Rectus Femoris	Hip	0.0302	0.0230	0	Knee	0.0347	0.0203	0

Table C.4: After moment arm correction

	Origin	X [m]	Y [m]	Z [m]	Insertion	X [m]	Y [m]	Z [m]
Illiopsoas	Hip	0.042	0.039	0	Hip	-0.006	-0.1419	0
Gluteus Maximus	Hip	-0.0822	-0.0391	0	Hip	-0.006	-0.1419	0

Table C.5: Muscle points for not calibrated muscles. Data from anybody models in Anybody-dir on CD-ROM

APPENDIX D

Muscle model results

This chapter gives all the figures that resulted from the muscle model verification. As described in section 5.1. The input data is available at figure 4.4 of section 4.3.3

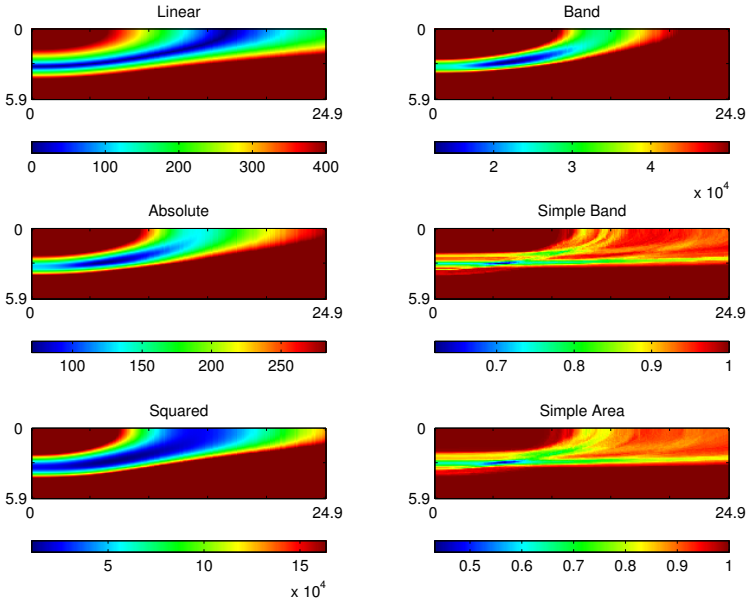

(a) Costs

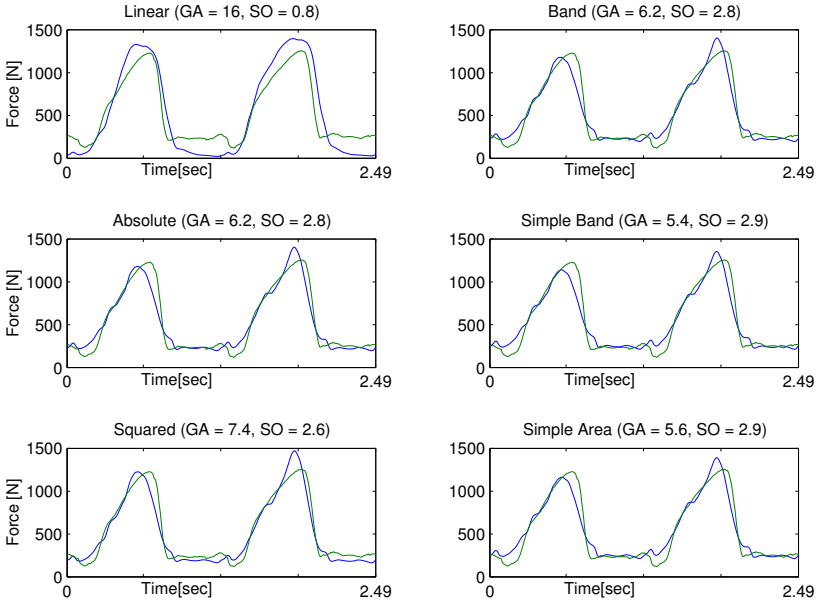

(b) Forces (blue = measured, green = predicted)

Figure D.1: $Bjorn_3$

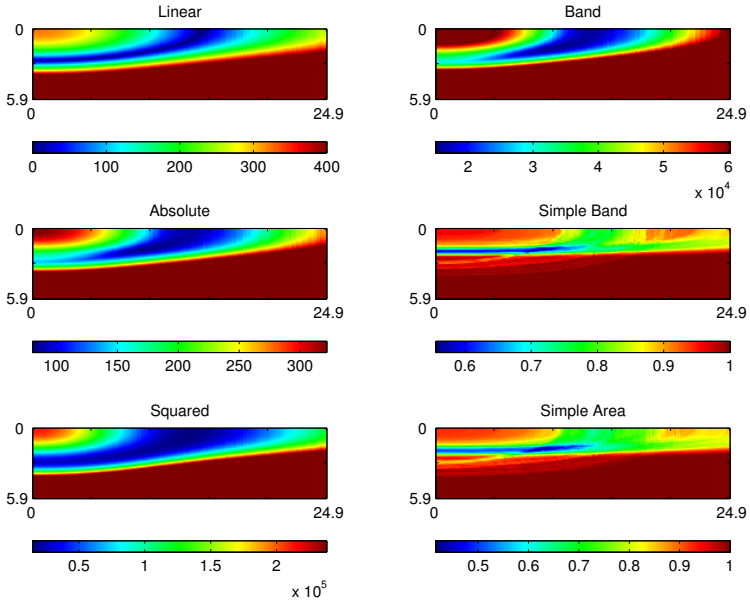

(a) Costs

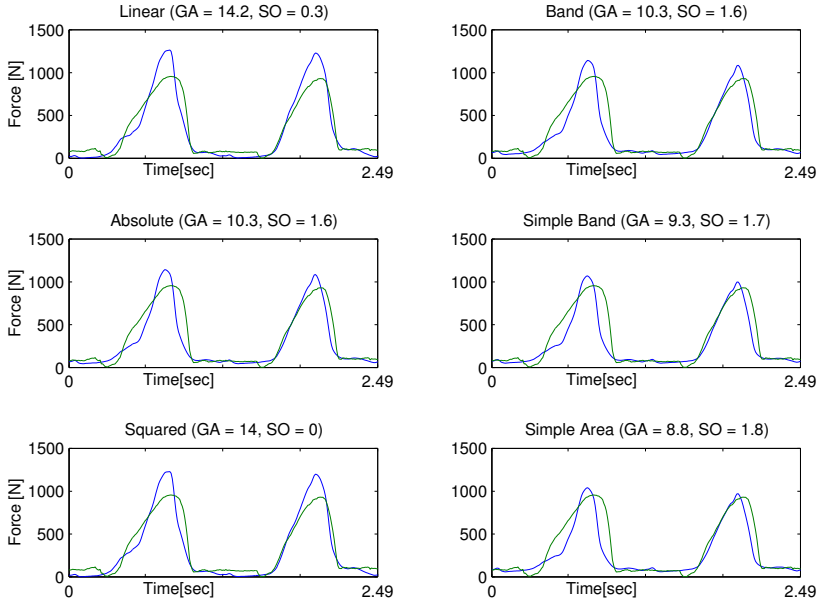

(b) Forces (blue = measured, green = predicted)

Figure D.2: $Bjorn_4$

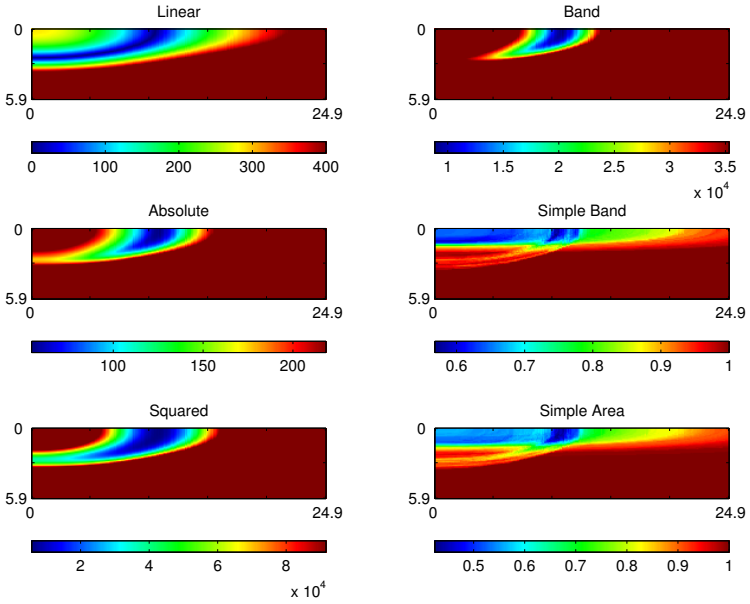

(a) Costs

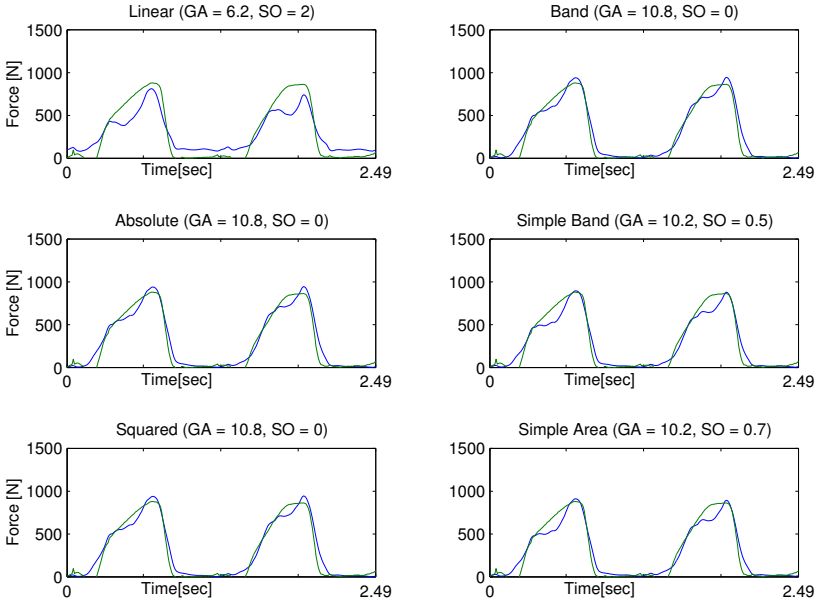

(b) Forces (blue = measured, green = predicted)

Figure D.3: $Bjorn_5$

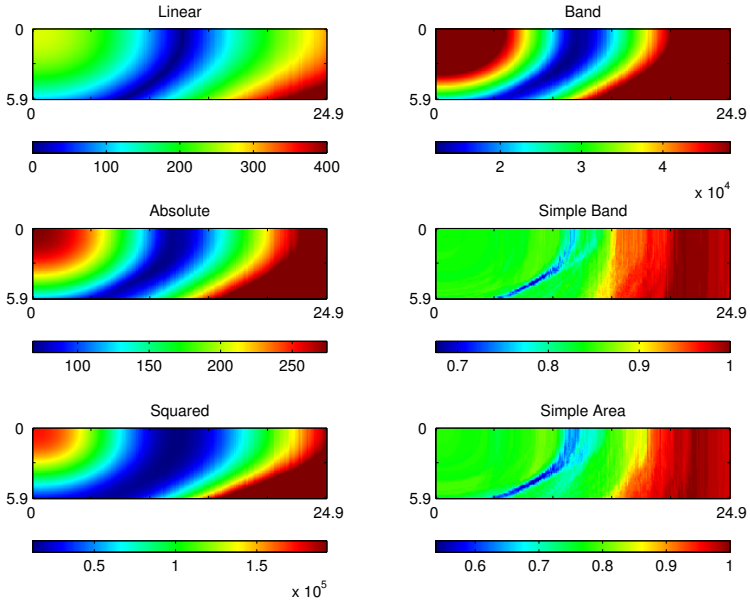

(a) Costs

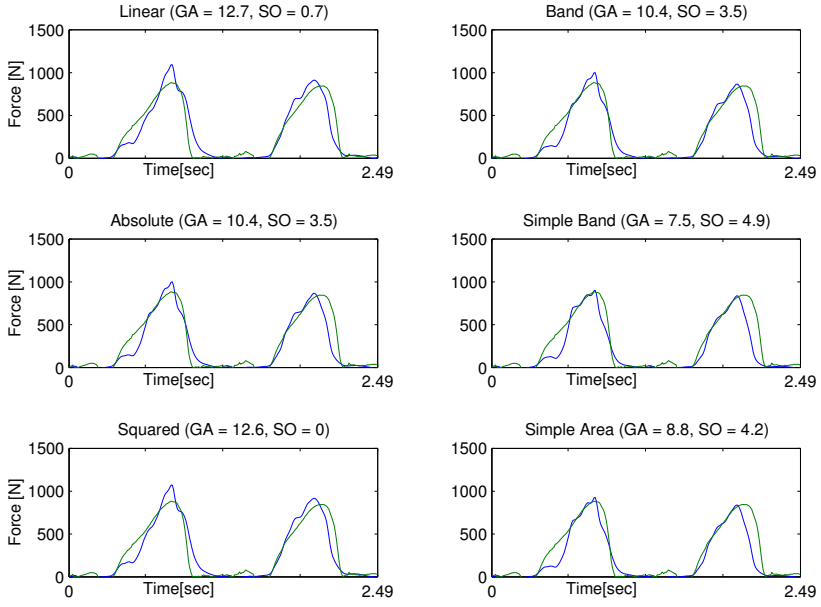

(b) Forces (blue = measured, green = predicted)

Figure D.4: $Bjorn_6$

List of Figures

List of Tables